Measuring the transmission yield of ultra thin membranes

by

Bram Looman

to obtain the degree of Master of Science
at the Delft University of Technology,
to be defended publicly on Tuesday February 11, 2020 at 10:00 AM.

Student number:	4251644	
Thesis committee:	Prof. Dr. Ir. H. van der Graaf,	TU Delft & Nikhef, supervisor
	Dr. C. W. Hagen,	TU Delft
	Dr. T. H. A. van der Reep,	TU Delft & Nikhef
	Dr. Ir. D. R. Schaart,	TU Delft

TNDO 20-02

TU Delft

Abstract

The goal of this research is to characterize thin membranes used as transmission dynodes (tynodes) for electron multiplication. A stack of tynodes could be used in a novel ultra fast soft photon counter. A combination of a charge sensitive TimePix1 CMOS chip and a pulsed electron gun were used as part of a setup deemed Tytest. The pixel chip was calibrated using a surrogate function that is fitted to the single pixel responses of 76 different pixels. The calibration is used to perform Transmission Secondary Electron Yield (TSEY) measurements on a 20 nm thick alumina membrane. The maximum TSEY value observed is 2.76 ± 0.64 for a incident energy of 1675 eV. The maximum TSEY value seems to be at higher incident energies which cannot be reached using our setup. A unexplained spread in electrons being emitted by the tynode is observed.

The second part of this research was to create a stack of tynodes which can be used to convert a single electron into a measurable signal. The goal is to stack the tynodes using a self aligning mechanism and measure the misalignment. A ZEISS Axio-zoom V16 light microscope in combination with two μm precision manipulators placed in a clean room at Nikhef in Amsterdam is setup in this research used to stack tynodes. The aim was to have a misalignment better than 5 μm, and this setup a misalignment of 4.1 ± 1.3 μm was measured. It's important to note that only the misalignment between two tynodes is measured, since no more were readily available.

Contents

1 Introduction

The need to detect soft photons (0.1 μm< λ <2 μm) [1] arises from the fields such as high energy physics, medical imaging and astronomy. Physical phenomena such as Cherenkov and scintillation radiation but also the light from many astronomical events are included in this range. The detection of such a photon starts by the creation of charge carriers in the detector. This can be in the form of a photo-electron or electron-hole pairs. The charge liberated by the ionization process of a single soft photon isn't enough to activate electronic circuitry. Therefore the charge has to be amplified, for instance with an electron multiplier.

1.1. Electron multiplier detectors

The first electron multiplier detector was the Photo Multiplier tube, which has been around since the 1930's. Next came Micro Channel plates and in the year 2000 Silicon Photo Multipliers came to the scene. Each of these detectors has its advantages and disadvantages which we will discuss here.

1.1.1. Photo Multiplier tube

The parts of interest in a Photo Multiplier Tube (PMT) are: the photo-cathode, multiple dynodes and the anode. When a incident photon hits a photo-cathode it may create a photo-electron. This photo-electron is accelerated to the first dynode which is put on a positive voltage with respect to the photo-cathode. When hitting the dynode the energetic photo-electron creates a few secondary electrons which get accelerated to the second dynode, which is at a higher voltage compared to the first dynode. This process repeats until there are enough electrons to create a measurable signal at the anode. A schematic representation of this process is shown in figure 1.1 on the left, on the right a picture of a PMT is shown.

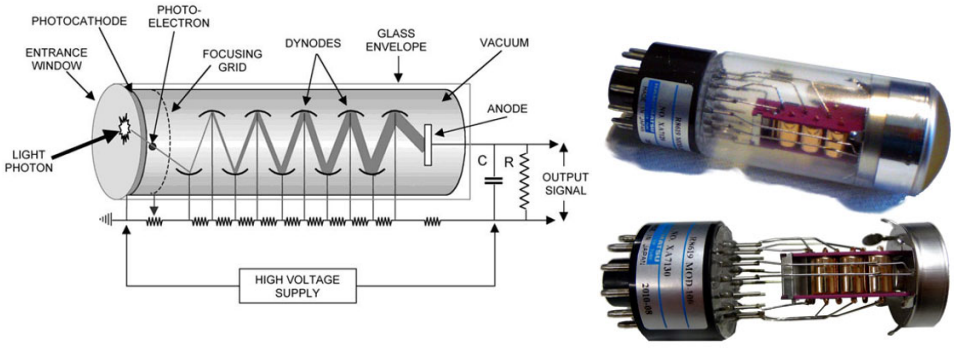

Figure 1.1: Left: schematic image of the process that leads to detection of a photon. Right: picture of a PMT. Image from [2]

PMT's are quite big and usually consist of only one channel and therefore lack spatial resolution in most cases. But there are PMT's with multiple channels where the spatial resolution can be in the mm range [3]. The time resolution is mostly determined by the variation in path length and speed of the electrons when travelling from the photo-cathode to the first dynode. The timing resolution of a PMT can be as good as

several hundreds of ps [4]. The efficiency is essentially the quantum efficiency (QE) of the photo-cathode, which can be around 10-40% depending on the photon wavelength and cathode material [3]. Due to the small chance of a thermal excitation of an electron in the photo-cathode a PMT has a low dark current, which allows certain PMT's to be used as photon counters. Unfortunately PMT's can't always operate in external EM fields as these fields will deflect the electrons which cause them to miss the dynodes.

1.1.2. Micro channel plates

A Micro Channel Plate (MCP) is usually a disk of highly restive material with small parallel pores as is shown in figure 1.2 on the left. The resistivity of the material allows a high potential difference to be put over the disk, which creates a electric field within the pores. When a electron enters a pore of the detector it will hit the wall at some point. The impact of this primary electron creates multiple secondary electrons which get accelerated by the electric field and hit the wall a little further which is shown in figure 1.2 on the right. This leads to a cloud of electrons at the anode which can be measured.

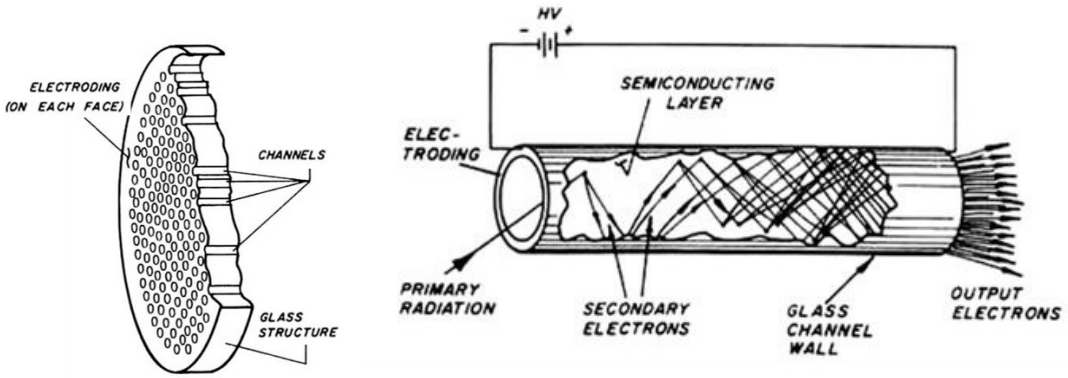

Figure 1.2: On the left, MCP with multiple channels. On the right, single channel. Image from [5]

The cloud of electrons arrives at the anode in a shorter time span compared to a traditional PMT, therefore a MCP usually has superior timing resolution [6]. The primary radiation (see figure) can be incident on different positions which limits the timing resolution. The geometry of these channels is typically a diameter of 6-50 μm [7] [8] and a length of 400 to 1000 μm. A MCP is able to operate in external EM fields since deflected electrons will still hit the channel walls at some point.

1.1.3. Single photon avalanche diodes

The basic building block of an avalanche photo diode (APD) is the diode, see figure 1.3. When a photon is incident on the depletion layer of the diode it excites a photo-electron to the conduction band creating a electron-hole pair. Due to the voltage over the diode electrons are accelerated to the positive side and holes to the negative side. By increasing this voltage the electrons will accelerate more during their journey to the electrode. At a certain voltage the accelerated electrons have sufficient energy to create new electron-hole pairs, which create again electron-hole pairs and so on. This voltage is referred to as the breakdown voltage and APD's usually operate a few volts above this voltage. So if one electron-hole pair is created it causes an avalanche of electrons which is essentially a charge pulse that can be measured.

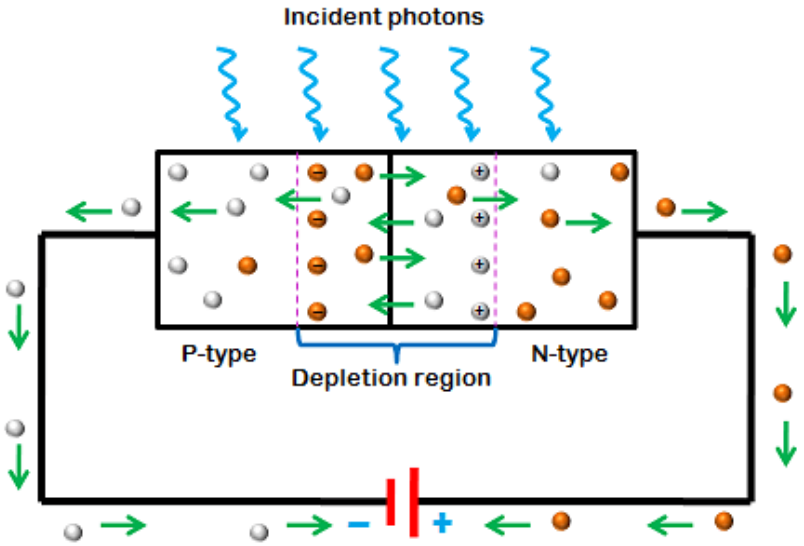

Figure 1.3: Schematic figure of a single APD. Image from [9]. When a photon is incident on the depletion layer it can create a electron hole pair. Electrons (red dots) and holes (white dots) are accelerated to opposite sides creating other electron hole pairs.

One pixel (or micro cell as in figure 1.4) consists of a APD connected with a quench resistor with some substrate material and contacts. The avalanche creates a current trough the resistor causing a voltage drop over the APD bringing the voltage below the breakdown voltage. The time it takes to recover is essentially the dead time of a pixel. By putting multiple of these pixels in a array the Silicon Photo Multiplier (SiPM) detector is created.

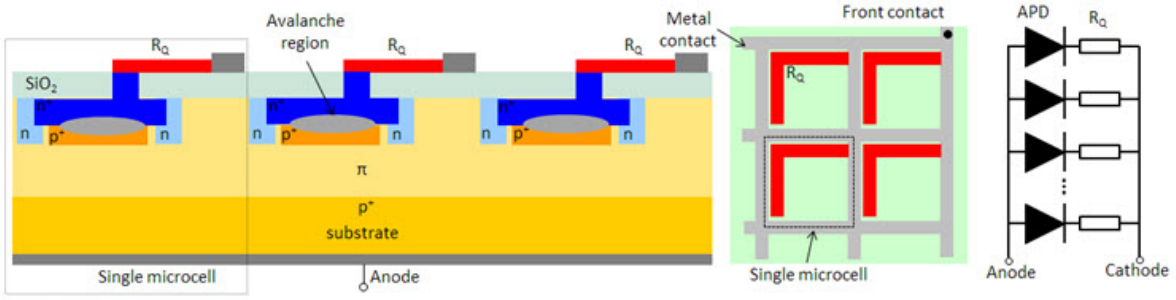

Figure 1.4: Schematic figure of SiPM. Image from [9]

The fill factor is the percentage of the detector surface that is sensitive to light. Here there are some considerations to take into account. First, there are usually around 100 to 1000 micro cells (or pixels) per mm^2. Each micro cell has some space around the active area for circuitry and to separate it from neighbouring micro cells. This non-active area is not dependent on the size of the active area so by increasing the micro cell size the fill factor increases, but the micro cell concentration decreases and thus the spatial resolution. furthermore by having a bigger active area, the photon interaction chance increases and so does the gain. So a bigger micro cell increases the photon detection efficiency. But the time it takes the micro cell to recover is again inversely dependent on the micro cell size. So to summarize: a larger micro cell means a higher fill factor and a higher detection efficiency but a longer recovery time and a lower spatial resolution[10]. And a smaller micro cell means a lower fill factor and detection efficiency, but a shorter recovery time and a higher spatial resolution. The timing resolution is determined by the variations in the avalanche process and small differences in the electronics [11]. The timing resolution of a single SPAD is in the order of several 100 ps [11], but this can be improved at cost of other parameters if timing resolution is of importance. Note the SiPM's are still under development and in recent years rapid improvements have been made [12].

Noise

A disadvantage of SiPM is the relatively high noise when compared to PMT's and MCP's. There are multiple sources of noise, the most important being the thermal excitation's. The charge carrier that initiates the avalanche can be due to a thermal excitation instead of a photon interaction. This avalanche is indistinguishable from a photon interaction so this will create a so called dark count rate. This dark count rate depends on the over-voltage (voltage above breakdown voltage) but is in the order of several tens of kHz per mm^2 of detector area (for 35 μm micro cells [10]). Another signal distortion source is after-pulsing, it's debatable whether this constitutes as noise because it's relation to an actual event. During the avalanche, electrons can be trapped in defects of the material lattice. After some time the trapped charge is released. If it is released within the recovery time not much happens. But the release time ranges from ns to a few μs which is longer than the recovery time[13]. Therefore the trapped electrons can initiate another avalanche which is again identical to photon induced avalanche. To reduce this effect SiPM's can be produced such that the concentration of defects is minimized. The final source of noise is cross-talk. During a avalanche accelerated charge carriers can emit photons. These photons can travel to neighbouring micro cells directly or escape the detector via the window and reflecting. This photon can again induce a avalanche which adds to the noise.

There are many solutions (which won't be discussed here) available for the problems stated here that can increase the performance for SiPM's which make SiPM's very useful detectors that are superior to PMT's and MCP's in many aspects. But due to the dark count rate SiPM's are not suitable as a single soft photon counters.

2

Tipsy

Eventually the goal of the project is to make a prototype of a new detector called the Timed Photon Counter (TiPC or Tipsy). If realized this detector will have excellent spatial resolution and efficiency. Tipsy will have similar noise levels as a PMT and will be able to operate in magnetic fields. But it's time resolution will be far superior compared to existing detectors. To understand how this performance is reached the working mechanism will be described.

2.1. Working mechanism

This detection process starts with the generation of one photo-electron due to a incident soft photon (0.1 μm< λ <2 μm) [1] on a photo-cathode. Next the photo-electron needs to be multiplied to create a measurable signal. This is done using transmission dynodes, which will be called tynodes in this report and they are the core of the electron multiplication mechanism.

2.1.1. The Tynode

A Tynode is made using Micro Mechanical Electronic Systems (MEMS) technology [1]. This way a ultra thin layer of several tens of nano meter thick is realised. If an energetic (up to ~ 1 keV) electron is incident on this thin film there are a number of electrons Y are emitted on the other side, here lays the core of the electron multiplication. This Y is called the Transmission Secondary Electron Yield (TSEY) and is used to quantify the performance of a tynode. If $Y > 1$ holds multiplication is achieved, the physics of this process is described in the Theory part. When multiple tynodes are stacked on top of each other a system where the number of electrons is multiplied by Y at each stage can be realized. An schematic image of this is shown in figure 2.1 where the multiplication process is visualized.

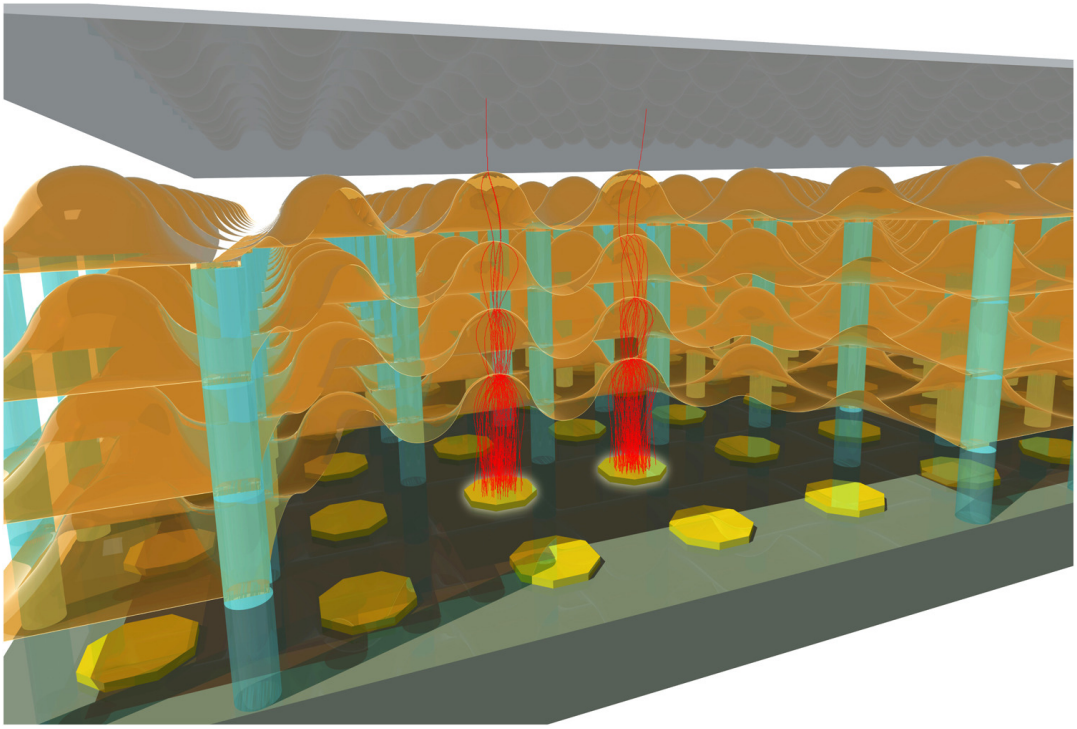

Figure 2.1: Schematic image of the basic working mechanism of Tipsy. The top grey plate represents the photo-cathode, the tynodes are orange plates (the shape is discussed later on) and the gold octagons are the anodes on which the electrons (red tracks) are collected. Image from [14], to get a sense of the dimensions: one column is 55 µm by 55 µm and the spacing between the plates is approximately ± 100 µm.

A photo-electron is accelerated towards and incident on the first tynode. As a result of this impact there are Y electrons emitted on the other side, so for N tynodes the total charge Q that is collected on the anode can be calculated with

$$Q = eY^N \tag{2.1}$$

where e is the electron charge. Between the tynodes the electrons must be accelerated to gain enough energy to induce the emission of electrons on the emission side. Therefore a potential difference in the order of 1 kV is put between each tynode. For a tynode spacing of 100 µm a electric field of $\pm 10^7 \frac{\mathrm{V}}{\mathrm{m}}$ is forced between the tynodes. If a value of 5 for Y can be realized a gain of $3 \cdot 10^3$ is reached with only 5 tynodes according to equation 2.1, which is enough to activate electronic circuitry.

2.1.2. Tynode shape

As can be seen in figure 2.1 the tynodes consist of and array of domes. This dome shape is advantageous for multiple reasons: first the curved shape increase the strength of the domes making them less vulnerable for mechanical stresses and easier to handle. The other reasons can be explained by how the dome shape influences the electric field. As can be seen in figure 2.2 on both sides of the dome the shape causes a electric field component towards the center of the dome. This causes the electrons to accelerate towards the center of the column creating a focusing effect.

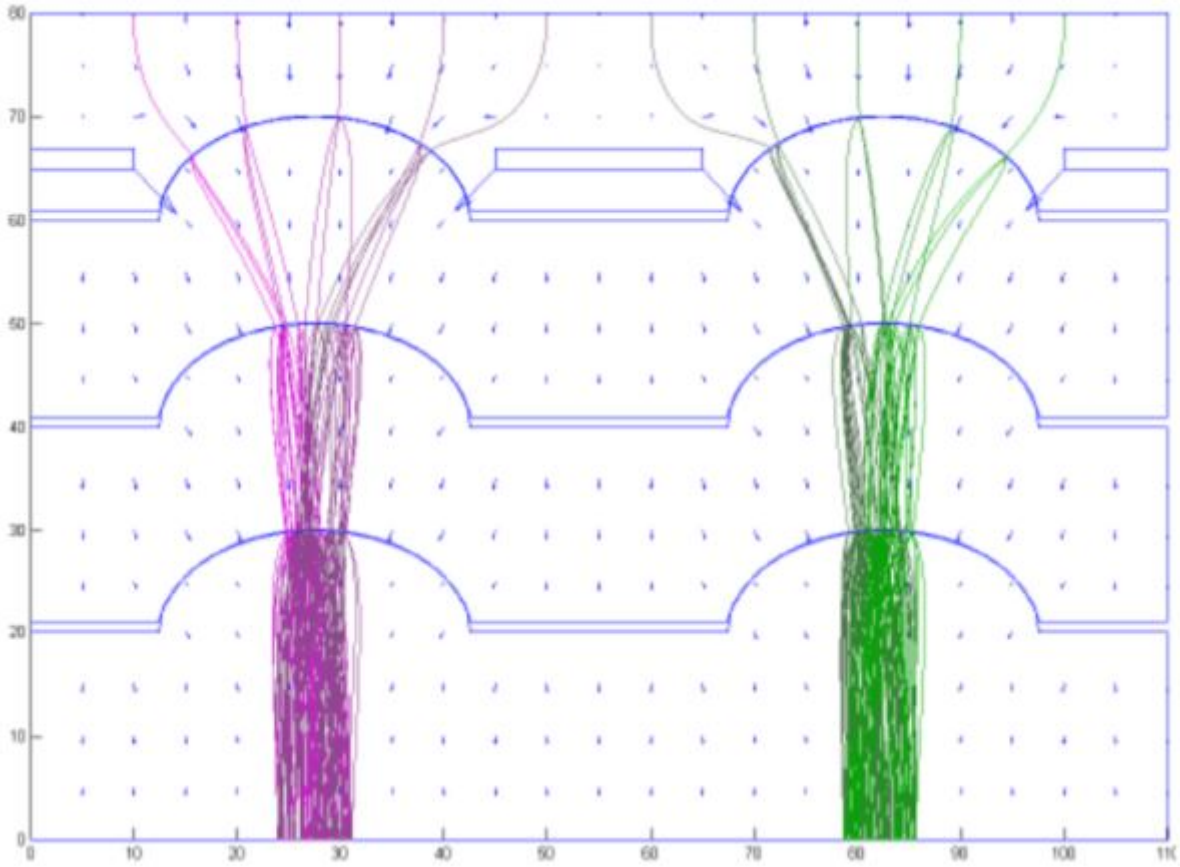

Figure 2.2: Schematic drawing of Tipsy to illustrate the effect of the dome shapes on the electron paths. Image from [1] where the spacing between dynodes is 20 µm with a potential difference of 150 V, the cone pitch is 55 µm and the incident electrons are created in horizontal steps of 10 µm along the cathode.

This focusing effect positively influences the fill factor by increasing the photo-cathode area in which emitted photo-electrons will cause a charge pulse on the anode. This can be seen at the top of figure 2.2 where a electron that would initially be incident on the support material between the domes is now incident on the active area of a tynode. Another advantage of this focusing is that all electrons travelling to the next tynode have more similar path lengths. This decreases the spread in arrival time on the anode which increases the time resolution.

2.1.3. TimePix

The final tynode is placed on top of a charge sensitive CMOS pixel chip which is called the TimePix chip. Using this pixel chip the amplified signal is measured and given a time stamp. In figure 2.1 this chip is shown as the gold octagons under the final tynode. The results in this report are obtained using a older generation of the TimePix chips, the TimePix1. The eventual prototype will have a TimePix3 (or newer) chip. The working mechanism of the TimePix1 chip is described in section 4.1.

2.2. Performance

When the Tipsy detector is realized it should have excellent performance and be superior to other soft photon counters. To make this statement plausible the expected performance and limitations will be discussed here.

2.2.1. Time resolution

The time resolution is very important in photon detectors. Since light travels at $3 \cdot 10^8$ m/s a small variation in time translates to a big variation in space. Therefore the accuracy of a Time of Flight (TOF) measurement is dependent of the time resolution. Currently photon detectors can reach time resolutions of a few 100 ps [4] [9] [5], but light still travels a few cm in this time which is too much in some cases. The time resolution

in Tipsy is determined by the variance in the time between the creation of the photo-electron and the time stamp of the measurement.

To get an idea of the order of this variance each step in the multiplication process is considered separately. The first step is the conversion from a photon to a photo-electron. This time frame is in the atto second range [15], which is so fast that the variance in this process is assumed to be negligible. However the place of creation does add time variance in when the photo-electron is emitted because the photo-electron needs to travel to the surface. The next step is the journeys from photo-cathode to the first tynode followed by the journeys from tynode to tynode. First the passing time t_p is calculated in the non-relativistic cases when assuming homogeneous electric fields with

$$t_p = S\sqrt{\frac{2m}{qV}} \tag{2.2}$$

where S is the distance the electron needs to travel, m and q are the electrons mass en charge respectively and V is the potential difference. For a distance $S = 100$ µm, and $V = 1$kV a passing time of 11 ps per tynode is realistic. For the entire system this leads to a total arrival time between the creation of the photo-electron and charge pulse on the anode of around 60 ps. Here two sources of time spread originate: first some electrons may be emitted with different energies causing them to have a difference in velocity. But the emitted electrons will have a energy of < 5 eV (see Theory part), which is small compared to the 1 kV potential difference and thus the increase in spread in arrival time caused by this effect is expected to be small compared to the total arrival time. And second, differences in emission angle and/or place will cause different path lengths. But due to the focusing effect discussed before the path length is expected to be similar for all electrons. This effect will increase the spread in arrival time, but again this increase will be small compared to the total arrival time. So to summarize, the difference in arrival time between: 1.the fastest electron with the shortest path length, and 2.the slowest electron with the longest path length, is small compared to the total arrival time. If the total arrival time is around 60 ps and the variance is small the time resolution should be far below 100 ps. Simulations by Hong Wah Chan confirm this [16] and show that the time spread in arrival time is even in the 5 ps range. Note these preliminary results are not yet published, but some results are already shown in appendix A. We expect that the biggest contribution to arrival time variance is due to the electrons travelling from the last tynode to the TimePix chip [6]. Since those electrons won't be accelerated as much the influence of angle and energy of the emitted electrons will cause a difference in arrival time. Another factor will be the time resolution of the TimePix chip, for a TimePix4 chip this is expected to be in the around 20 ps.

2.2.2. Spatial resolution and fill factor

The spatial resolution is determined by the pixel size. The current TimePix1 chips have pixel arrays of 256 by 256 pixels which are 55 µm by 55 µm in size, which sets the spatial resolution at $\frac{55\,\mu m}{\sqrt{12}} \approx 16$ µm.. The active area or fill factor is determined by the part which the domes occupy on the first Tynode. For 30 µm diameter domes which are spaced 55 µm apart the active area will be at least ±30%. However this is increased due to the focusing effect of the first tynode as discussed before.

2.2.3. Performance in magnetic fields

A external magnetic field will deflect the electrons changing their path as can been seen in figure 2.3. But due to the strong electric field between the tynodes Tipsy is still able to function when force exerted by the electric field is significantly stronger than the Lorentz force due to the external magnetic field.

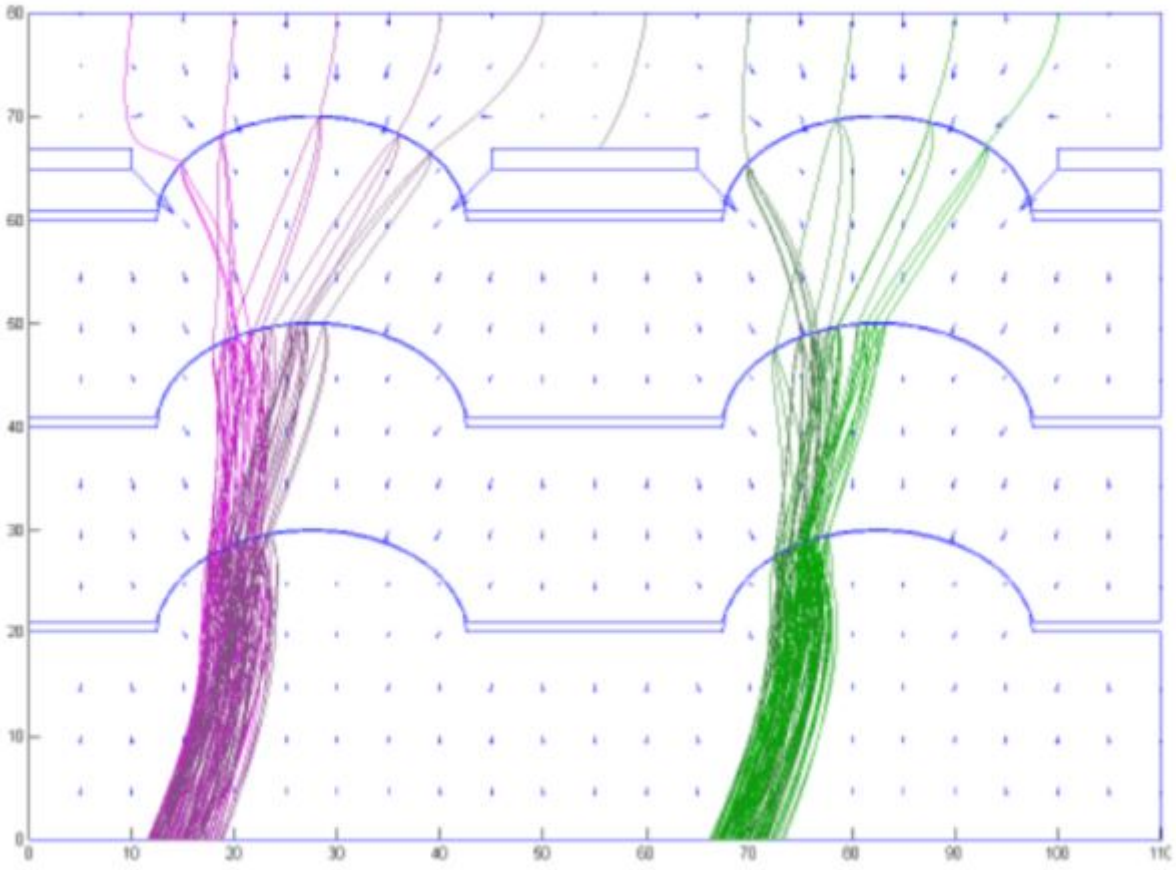

Figure 2.3: Similar simulation result as before but now for a magnetic field of 1 Tesla, image from [1].

A magnetic field can increase the differences in path length which negatively influences the time resolution. However the TimePix should still be the determining factor. There are limits on the strength of the external magnetic field: at some point the electrons are deflected too much and don't hit the anode. This effect becomes worse as the number of tynodes increases which is shown in figure 2.3. The limit on the strength of the external magnetic field will be determined by a combination of the potential difference and distance between the TimePix chip and the last tynode.

3

Theory

A essential part of the Tipsy detector is the transmission dynode or tynode. When one electron is incident on a tynode multiple secondary electrons should be emitted on the opposite side. The mechanism responsible for this secondary electron emission (SEE) will be discussed in this chapter and the properties that influence the SEE will be identified.

3.1. Secondary electron emission

Most literature on SEE discusses the Reflection Secondary Electron Emission (RSEE), where the secondary electrons are emitted on the side were the primary electron was incident. For a tynode the interest is in the Transmission Secondary Electron Emission (TSEE), where the electron emission is on the opposite side of the incident electron. The physics of RSEE and TSEE is similar and can be described in three steps: generation, transport and escape. To quantify the SEE of a material the yield is used. The yield is defined as the average number of electrons emitted by the material per incident electron. In this report we will talk about the Reflection Secondary Electron Yield (RSEY) and the Transmission Secondary Electron Yield (TSEY)

3.1.1. Generation in material

When a primary electron (PE) enters a material it can lose energy by collision with the lattice electrons. When colliding with a lattice electron some kinetic energy will be transferred causing the lattice electron to be excited from the valence band to the conduction band, creating a electron hole pair [17]. Here we will assume that the PE is incident perpendicular on the surface, such that the depth x of the PE is also the depth in the in the material. The amount of energy that the PE loses between x and $x + \Delta x$ is proportional to the number of electrons excited to the conduction band. This process can be described by [18]

$$n(E_0, x) = \frac{-1}{\epsilon} \frac{dE}{dx} \tag{3.1}$$

where $n(E_0, x)$ is the number of internally generated SE at depth x for a PE with energy E_0, ϵ is the average energy it takes to create a electron hole pair and $\frac{dE}{dx}$ is the energy loss of the PE. If a SE has sufficient energy it can also create electron hole pairs. This leads to an interaction volume as shown in figure 3.1. Here it's illustrated where the secondary electron (SE) and the Backscattered electrons (BSE) are created.

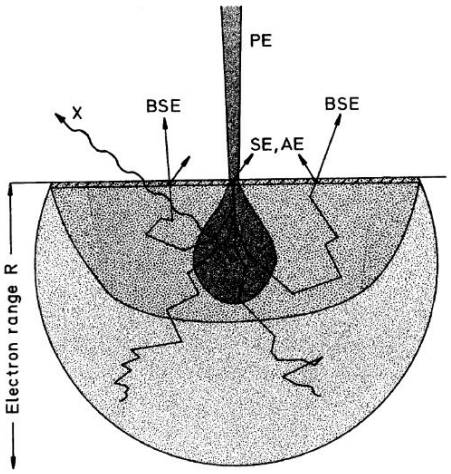

Figure 3.1: The interaction volume of an PE beam with normal incidence to shown where SE, BSE, AE and X are created. Image from [19].

The energy of SE is by convention smaller than 50 eV, and for BSE greater than 50 eV [19][20]. SE are usually created by inelastic collisions which excites electrons to the conduction band. BSE have higher energies and undergo multiple scattering events which can induce other SE. When a electron is kicked out of one of the inner shells of an atom an electron from a higher shell will fall in creating a X-ray with the energy of the energy difference of the two shells as $h\nu = E_{outhershell} - E_{innershell}$. But this energy can also be transferred to another electron bound to the atom creating an Auger electron (AE). The Auger electrons (AE) and X-rays (X) are neglected from now on since they don't serve any purpose in this report. These events stop when the PE has lost almost all of it's energy and can't create another electron hole pair, the corresponding depth is called the penetration depth R which can be calculated by

$$R = -\int_0^{E_0} \frac{dx}{dE} \cdot dE. \tag{3.2}$$

The energy loss $\frac{dE}{dx}$ isn't constant, the rate at which the PE loses energy is dependent on its own energy. This can be explained by the velocity of the PE, when a PE is incident on a material the velocity is relatively high which leads to a small time to interact this lattice electrons. When the PE is slowed down the interaction time increases and so does the energy loss. The energy loss can be described using a power law [18]

$$\frac{dE}{dx} = \frac{-A}{E^{n-1}} \tag{3.3}$$

where A is a constant and n is the power. Since the energy loss is higher closer to the penetration depth more SE are generated deeper in the material. Solving equation 3.3 for a PE with energy E_0 at $x = 0$ an expression for E is obtained

$$E(x)^n = E_0^n - Axn \tag{3.4}$$

which describes the energy of the PE at a certain depth. To find the penetration depth we can insert equation 3.3 into equation 3.2 to obtain

$$R = \frac{E_0^n}{An} \tag{3.5}$$

which gives the penetration depth of the PE. The same result can be obtained by solving for x if $E(R) = 0$ in equation 3.4. For the tynodes it's important that they are thicker than the range of a PE such that all the energy is deposited in the material. But if the tynodes are too thick the internally generated SE cannot reach the surface and stay inside the material.

3.1.2. Transport through material

Once a lattice electron is excited from the valence to the conduction band it can no longer feel the positive charge of the atom core. This means it can travel freely through the material. For metals the conduction band is filled with other electrons, which means the internally generated SE mainly loses energy by collisions

with other electrons in the conduction band. The SE will lose energy quickly and isn't able to diffuse far from the point of creation. For semiconductors and insulators the SE in the conduction band mainly loses energy by collisions with valence electrons (which can again excite the valence electron to the conduction band). After the SE energy is below the band gap of the material it can't scatter inelastically with valence electrons. The SE loses energy by collisions with lattice vibrations which cause an energy loss in the order of kT per collision [21]. This means the SE can diffuse for bigger distances compared with metals, which is why semiconductors and insulators usually have higher yields compared to metals. The chance of a internally generated SE diffusing over a distance r can be described using a absorption coefficient α with [18]

$$P_{travel}(r) = \exp(-\alpha r). \tag{3.6}$$

This means that a greater portion of the created SE reach the surface if they're created close to the surface, which is a effect that works adversely with the increased creation of SE at higher depth for RSEE. For a tynode these effects could work together to create a higher yield. A schematic drawing of this is given in figure 3.2.

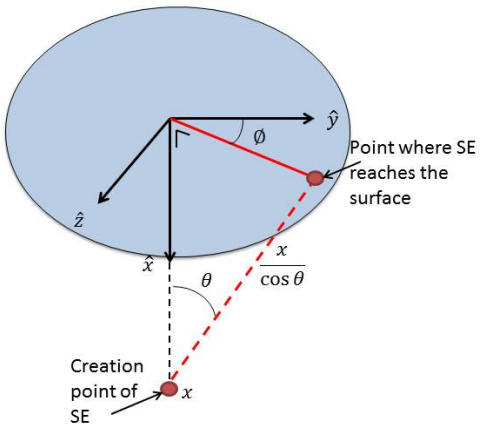

Figure 3.2: Image that shows the transport problem for a SE, image recreated from [20].

Using the coordinates defined in this image it's possible to define the chance of a internally generated SE diffusing to the surface. If we assume the SE are created isotropic and SE travel only in a straight line (scattering of SE is ignored) the chance of an SE created at depth x reaching the surface is [20]

$$P(x) = B\int_0^{2\pi}\int_0^{\pi/2} \exp(\frac{-\alpha x}{\cos\theta})\sin\theta d\theta d\phi \tag{3.7}$$

where B is a constant and the angles can be found in figure 3.2. It's important to note that this chance only depends on the distance to the surface in this derivation, both for TSEE and RSEE. In reality there will probably be more forward scattering which is ignored here. If the SE reaches the surface it needs to escape to vacuum

3.1.3. Escape to vacuum

For tynodes it's important to have a high TSEY to have fast electron multiplication with as little tynodes as possible. Therefore it's important that SE can easily escape the material. When the SE arrive at the material vacuum interface they have to overcome a potential barrier to escape. In insulators and semiconductors this potential barrier is the electron affinity (EA) and is shown in figure 3.3 (for metals this is the work function). When a SE reaching the surface does not have enough energy to overcome the EA, it will be reflected back into the material.

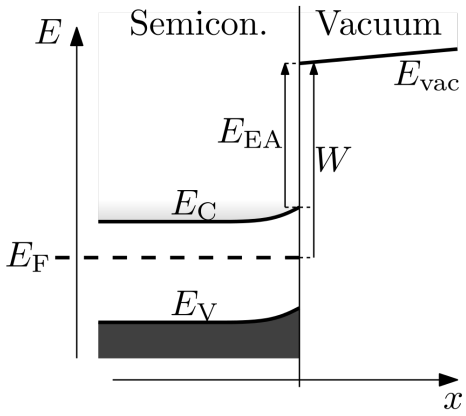

Figure 3.3: Band diagram of semiconductor vacuum interface, showing the electron affinity E_{EA} which is the difference between the conduction band minimum E_C and the vacuum energy E_{vac}. The work function W, the Fermi energy E_F and the valence band energy E_V are also shown. Image from [22].

In the case of negative electron affinity (NEA) where $E_{vac} < E_C$ these electrons will be emitted in the vacuum. The NEA can be achieved by surface treatment on the emitting surface [22]. This will greatly improve the transmission yield.

3.1.4. Extracting field

When en external electric field is present at the surface of a material it influences the potential barrier. When this field is too high (10^9 V/m for metals [23]) it will induce emission of electrons without the need for a PE, which is called cold emission. This is not advantageous for Tipsy because this will cause dark count if this happens in the photo cathode, and unwanted currents if it happens in a tynode. Before the point of cold emission is reached, there is an area of sub-threshold field emission (SFE), in which the TSEY is enhanced by the electric field but there are no field emissions. It is shown that SFE can increase the TSEY yield significantly [24][25]. This is very advantageous for Tipsy because this will increase the the TSEY and the fields are already present due to the voltage difference between tynodes.

3.2. Emission curves

There are two main effects to consider: higher energy electrons will generate more SE on average deeper in the material. And that the further a SE need to travel before reaching the surface the less chance it has of reaching this surface.

3.2.1. RSEY curve

A example of a RSEY measurement is shown in figure 3.4. Here three energies are defined: first the energies where $\delta = 1$ at E_I and E_{II} such that $E_I < E_{II}$. This defines three regions: the first region at $E_0 < E_I$ is where the SE are created close to the surface so relatively many SE can escape, but not enough SE are created for a RSEY above 1. In the region where $E_0 > E_{II}$ there are more SE created, but they are created at such depths that most of them can't escape causing again a RSEY below one. In the region $E_I < E_0 < E_{II}$ more electrons are emitted from the surface that are incident on the surface leading to a SEY above 1, the maximum yield δ_m is in this area.

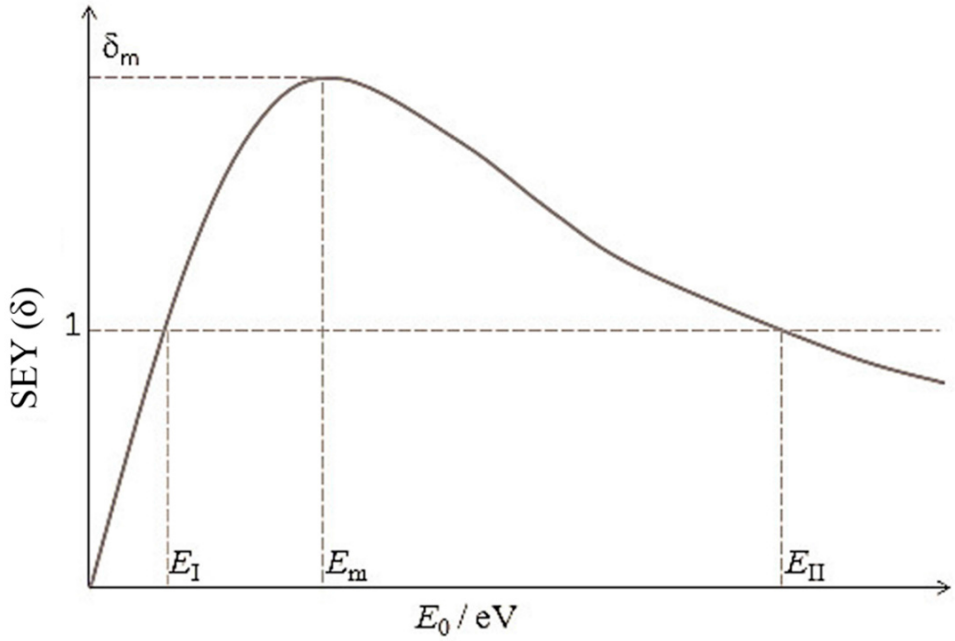

Figure 3.4: RSEY curve as function of PE energy, note the energies E_I and E_{II} where the SEY equals one and the E_m where the SEY is maximum. Note here is assumed the $\delta_m > 1$, which is not true for all materials. Image from [22].

In the first two regions ($E_0 < E_I$ and $E_0 > E_{II}$) negative charging will occur. Electrons will accumulate in the material causing a increase in the RSEY. In the third region where $E_I < E_0 < E_{II}$ holds, positive charging occurs. Therefore electrons will need to have more energy in order to reach the surface and escape, which causes the RSEY to decrease. If the charging effect is too severe, at some point the yield will become unity for both cases.

In other literature the TSEY and RSEY curves showed similar behaviour [6]. But a difference between the RSEY and TSEY is that at higher energies the PE won't deposit all its energy in the material and go through. At this point a drop in SE will cause a decrease in SEE. But in our setup the PE will also contribute to the charge accumulated in the pixel chip, and thus be measured as a SE which it is not. We hope to be able to define again three regions for the TSEY curve with a maximum yield and corresponding energy.

3.2.2. Charging of insulators and dead time

A tynode should have a yield > 1, which means more electrons leave the material than are incident. Since tynodes are made from non conductive materials this will cause the tynode to charge up positively. The positive charge will decrease the yield and if the charging is too severe the yield will become unity, which means no electron multiplication. Therefore a countermeasure is taken in the form of a thin conductive layer (4 nm TiN [26]) on the incident side of the tynode. The time it takes before the excess charge Q has disappeared can be considered the dead time of the electron multiplication system, because during this time the TSEY will be lowered.

4

TyTest Set-up

The eventual goal of the Tytest setup is to do TSEY measurements on Tynodes, and try to achieve electron multiplication. Although these measurements are also possible in a SEM [6] [16], in Tytest the measurements are performed with a pulsed electron beam in combination with the TimePix1 chip. This will represent the working mechanism of the Tipsy detector better compared to the DC measurements in a SEM. Using this method it's also possible to investigate effects as extracting fields and charge up using a TimePix1 chip. Because of the sensitivity of the TimePix1 chip for a few thousand electrons [27] [28] and the ability to sent multiples of 20 ns electron pulses the TyTest setup is a very useful tool for TSEY measurements and eventually full characterization of the tynodes. The TyTest setup consists of the TimePix chip and the Electron gun as discussed, two pulse generators, a oscilloscope and a source meter. In this chapter we will discuss how these instruments work together to perform measurements in TyTest.

4.1. The TimePix chip

There are four TimePix1 chips mounted on a vacuum flange which are simultaneously been read out by a computer. The TimePix chip was used in combination with the readout and control software program SoPhy (Software for Physics). All settings must be controlled using SoPhy. The layout of a single TimePix1 chip is shown in figure 4.1. One TimePix1 chip consists of a matrix with 256 by 256 pixels, each pixel has a size of 55 µm by 55 µm. This leads to a active area of 1.982 cm^2 which is spanned by 16120 µm by 14111 µm making 87 % of the chip's surface active [28].

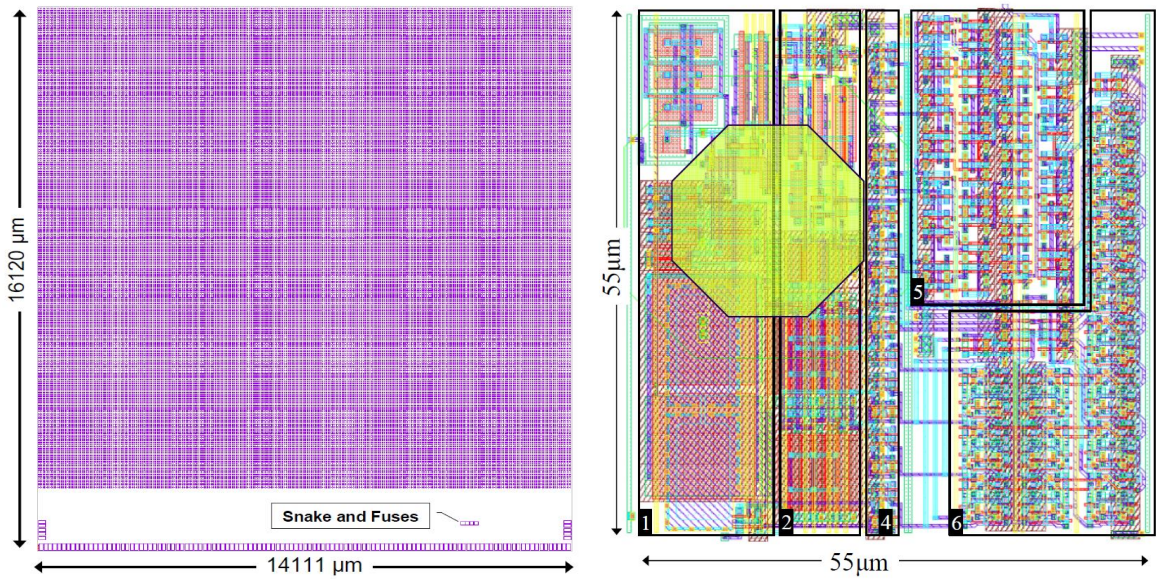

Figure 4.1: Left: Timepix layout with 256 by 256 pixels and a non sensitive part on the bottom. Right: Single pixel where 1: pre-amplifier, 2: Discriminator, 4: configuration latches, 5:BWD and 6: shift register and overflow control. Images from [28]

As can be seen on the right the octagonal input pat is not the size of the pixel. For three of our four TimePix chip's a layer of copper was added over this input pat effectively increasing the size of the input pat. Those chips are the only ones used for measurements in this report.

4.1.1. Pixel circuitry

The schematic overview of the analog part from a single pixel can be seen in figure 4.2. The input pad is where the charge is collected which changes the voltage of the input pad. This voltage is amplified by the Preamp and compared to a threshold (THR) with a discriminator. When the voltage is higher than the THR voltage the discriminator is activated.

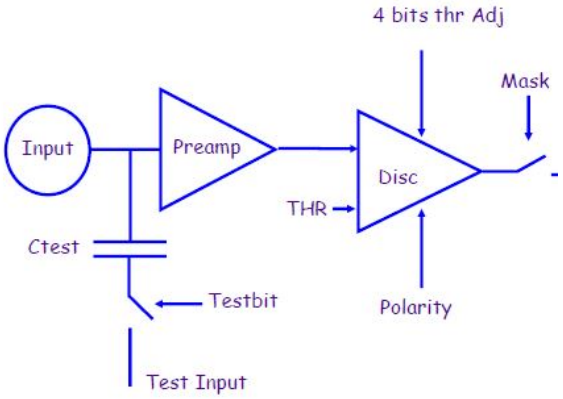

Figure 4.2: Analog part of single pixel, image from [28].

The pixel chip has three clock settings: 100 MHz, 50 MHz and 10 MHz. When the discriminator output is high the selected clock counts into a 14 bit shift register. The maximum count is 11810, which sets the maximum value each pixel can have. When a measurement starts the shutter opens, during this time the clock can count into the register. After the shutter closes the chip is read out and a new measurement can be started. There are three modes the TimePix chip can measure in.

counting mode

In this mode the TimePix1 chip counts the times the threshold is crossed. For experiments with a pulsed electron gun this is expected just to be the number of pulsed within the shutter time. This mode should be used when the number of hits is of interest. It's not possible to say anything about the arrival time other dan it was during the shutter time. The amount of charge collected on the pixel stays also unknown in counting mode.

Time of Arrival (ToA) mode

In this mode the TimePix1 chip starts counting when the threshold is crossed for the first time. It stops counting when the shutter closes and thus the data is going to be read out (see figure 4.3). If we assume the time when the shutter closes is known accurately it is possible to compute when the charge arrived at the pixel. This mode should be used when the best time resolution is wanted. It's not possible to register multiple hits during the shutter time or to get information about the amount of charge other than it was enough to cross the threshold.

Time over Threshold (ToT) mode

In this mode the TimePix1 chip registers the time the voltage in a pixel is over the threshold, see figure 4.3. This is a measure for how much charge is collected on the pixel, since more charge will lead to a longer time above the threshold. Unfortunately this is not a linear dependence and the TimePix1 chip needs to be calibrated before charge measurements can be done correctly. In this mode the arrival time and the number of events remain unknown.

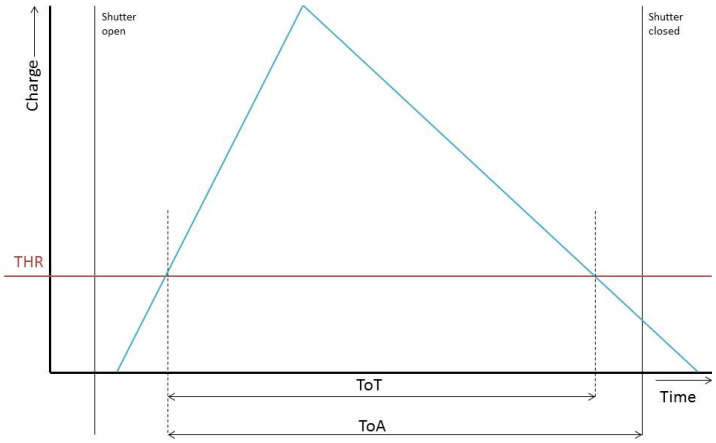

Figure 4.3: Schematic image to compare ToT measurements with ToA measurements

For each of these modes, after around 100 ns after the threshold is reached the a current starts to drain the charge collected on a pixel. This leads to a decrease in voltage on the pixel. After the charge is drained the pixel is ready for the next event, if this is allowed by the selected mode. To make sure all pixels show similar behaviour its necessary to have equal threshold levels in each pixel.

4.1.2. Threshold equalization

There will be some pixel to pixel variations due to mismatches in local transistor threshold voltages and currents [29]. These variations are compensated by a so called threshold equalization procedure which is performed by SoPhy. It isn't possible to adjust the threshold of each pixel separately. Per chip there is a common THL and a THS value. The THL value represents the minimum threshold (THR value) of all pixels on a chip. The THS value represents the spread between pixels on the chip. Each pixel is assigned a number from 0 to 15, which is called the threshold adjust or TH_{adj} in equation 4.1. The TH_{adj} is the only value that is pixel dependent and this means each pixel has one of 16 different threshold settings. The THL and THS values are also determined during the equalization but are the same for all pixels on the chip. The formula to calculate the threshold for pixel $[i, j]$ is

$$THR[i, j] = THL + TH_{adj}[i, j] * \frac{THS}{15} \tag{4.1}$$

where the units of THR, THL and THS are "threshold points" and one threshold point represents ~25.4 electrons [27]. This does not mean that the TimePix1 is sensitive for 25.4 electrons. SoPhy converts the THR setting to a physical voltage which is the input for the discriminator as is shown in figure 4.2. Here we can see that the discriminator compares the output of the preamplifier to the set THR value. The equalization is performed in counting mode so if the THR voltage is within the noise distribution of the preamplifier output, many counts will be registered. When the THR value is equal to the DC level of the preamplifier output most counts will be registered, and this is how SoPhy knows where the DC level is. To find the region where the THR voltage is within this spread, SoPhy scans through the possible THR values by changing the THL value of the chip from its maximum value to its minimum value. This scanning is done twice: once for the minimum THR value where $TH_{adj}[i, j] = 0$ and once for the maximum THR value when $TH_{adj}[i, j] = 15$ (see equation 4.1). These results are shown in figure 4.4 where the red and blue curves represent the results for $TH_{adj}[i, j] = 0$ and $TH_{adj}[i, j] = 15$ respectively.

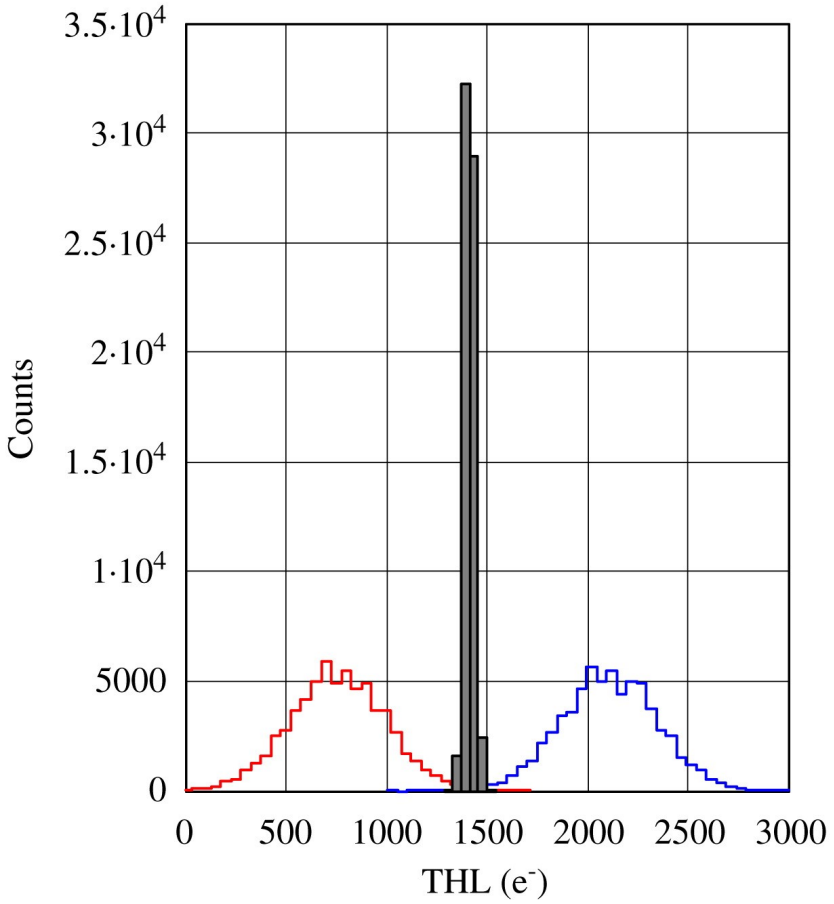

Figure 4.4: This figure shows the results of an equalization for another TimePix chip as an example to explain the equalization procedure. Image from [29]

The histograms are the number of counts registered over the whole chip for a certain THL value. If the mean of the noise distribution (DC level) is equal to the set THR value the maximum number of counts will be registered. Note that the distance between the two centers of these distributions represent the THS value from equation 4.1. Values from this figure will be referenced below as an example and have no meaning in this report. The peaks of the distributions are around ~750 electrons for $TH_{adj}[i,j] = 0$ and ~2100 electrons for $TH_{adj}[i,j] = 15$. Therefore SoPhy is going to try to get all THR values as close as possible to $\frac{750+2100}{2} = 1425$ electrons. For each pixel SoPhy chooses the $TH_{adj}[i,j]$ such that the THR value is as close as possible to 1425 electrons. How this process works is explained for two example pixels.

Our first pixel is in the center of the distribution. The maximum number of counts is ~750 electrons for $TH_{adj}[i,j] = 0$ and ~2100 electrons for $TH_{adj}[i,j] = 15$. SoPhy divides the range from 750 electrons to 2100 electrons into 16 steps and chooses the $TH_{adj}[i,j]$ that makes the THR closest to 1425 electrons. So the $THR[i,j]$ value will be round$(\frac{1425-750}{2100-750} * 15) = 8$.

Our second pixel doesn't behave as an average pixel and has a maximum number of counts on the left side of the distributions. The maximum number of counts are at ~250 electrons for $TH_{adj}[i,j] = 0$ and ~1600 electrons for $TH_{adj}[i,j] = 15$. SoPhy divides the range from 250 electrons to 1600 electrons into 16 steps and chooses the $TH_{adj}[i,j]$ that makes the THR closest to 1425 electrons. So the $THR[i,j]$ value will be round$(\frac{1425-250}{1600-250} * 15) = 13$.

During a equalization this is done for all pixels. In figure 4.4 the grey bars in the center represent the THR values after the equalization. Its clear to see that the pixels have more similar thresholds after the equalization. If better sensitivity is required, pixels that behave far from the average can be deactivated to minimize the THS. For the purposes of this report deactivating pixels isn't desirable because all the charge deposited on a deactivated pixel is not taken into account.

4.2. The Electron gun

For this experiment a ELG-2 Electron Gun with a ELGS-1022 Power Supply system was used. A schematic overview is shown in figure 4.5 where different voltage sources are shown. The manufacturer is *Kimball Physics* [30] and with this system parameters as beam energy, current, focus and deflection can be controlled separately. All settings can be adjusted on the front panel of the ELGS-1022 Power Supply system. But they can also be controlled by connecting the system with a zero modem cable to a computer. The Electron gun system can now be controlled using a programming language, Python in this project. This allowed the measurement process to be automated.

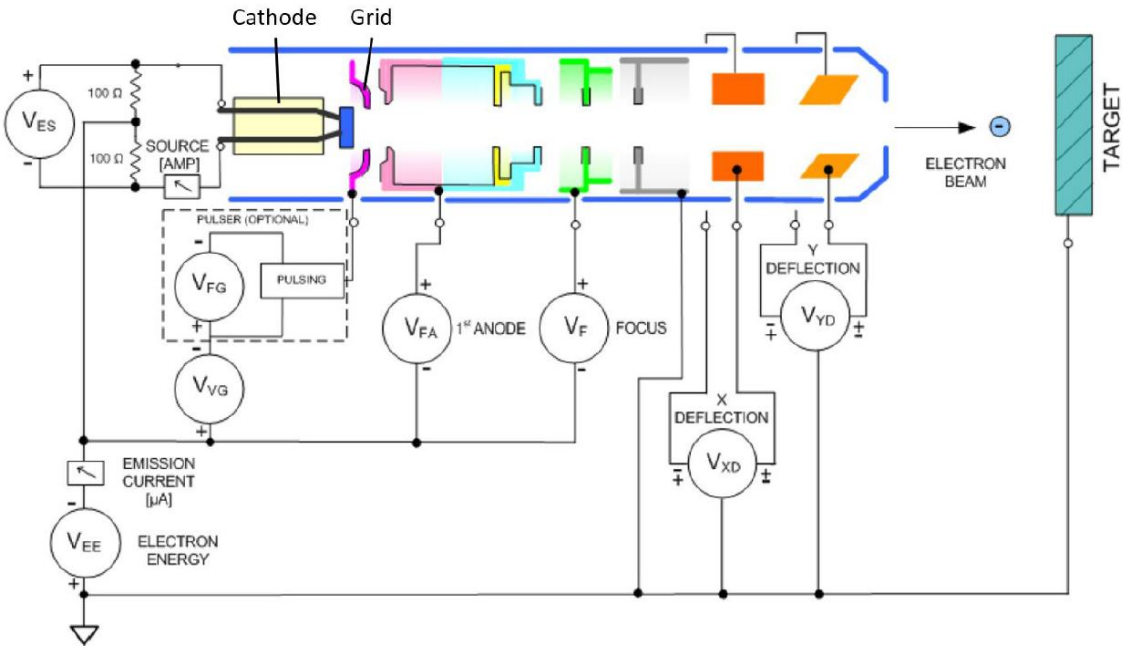

Figure 4.5: Schematic overview of the working mechanism of the electron gun, image from [30]

The electrons leave the gun at ground potential, therefore the voltage of the cathode must be set at minus the accelerating voltage V_{EE}. By increasing the source voltage V_{ES} the current trough the cathode will flow which will increase the temperature of the cathode, without changing the cathode potential. By increasing the voltage of the 1st anode V_{FA} the electrons will be pulled from the cathode and accelerated to the anode. For pulsed mode there will be a constant negative voltage V_{FG} on the grid which suppresses the electrons so no electrons leave the cathode. By pulsing with a positive voltage over V_{VG} the grid potential will increase allowing the electrons to escape from the cathode. Changing the focus potential V_F effectively changes the spot size and by changing V_{XD} and V_{YD} the beam is deflected in the x and y direction respectively. An overview of the ranges can be seen in table 4.1.

Source	Range
Cathode voltage V_{EE}	-1V to -2kV @ 20μA
Grid V_{VG}	0V to 50V
First anode V_{FA}	0V to 200V
Focus V_F	0V to 2kV
Source V_{ES}	0V to 3V @ 3A
X deflectionV_{XD}	-150V to 150V
Y deflection V_{YD}	-150V to 150V

Table 4.1: Table with ranges of the electron gun settings, grid and focus and anode are given relative to V_{EE} [30].

The cathode is a thermionic emitter and made of Tantalum which is mounted on tungsten filament wire that is heated from the voltage source V_{ES}. The Tantalum disc should be as smooth as possible to ensure a

constant emission across the surface. To increase the electrons leaving the cathode and thus increasing the current there are two options. One is to increase the cathode temperature and the other is to increase the extracting field. Here we can distinguish two modes of operation.

Temperature limited mode

Here the temperature is relatively low en the 1st anode voltage is relatively high. This leads to an exponential dependence of the current as a function of temperature [30]. In this mode small temperature fluctuations will cause relatively big fluctuations in the electron gun current. All available electrons will be extracted by the 1st anode, and the cathode temperature determines how many electrons are available.

Space charge limited mode

If the temperature is relatively high and the 1st anode voltage is relatively low the electron gun operates in Space Charge limited mode [30]. Due to the high temperature the electrons in the cathode have relatively high energy. This makes it easier to cross the vacuum barrier. With a small voltage on the 1st anode a lot of electrons can be extracted from the cathode. This means the anode voltage controls the emission current. Since the anode voltage is relatively more stable than the temperature of the cathode operating the gun in Space Charge limited mode will give a more constant emission current. This mode wasn't usually used because due to the high cathode temperature the degradation of the cathode will be accelerated.

4.2.1. Current drift

Current measurements can be performed using a Faraday cup. This is a copper hollow cylinder with a opening on one side. By putting the opening in front of the electron beam all electrons will enter this cylinder. Due to its geometry SE's and BSE's cannot escape the cylinder and will be absorbed. To make sure all electrons are absorbed the Faraday cup is put at a positive potential of 200 V. By measuring the current from the Faraday cup the current of the electron gun can be measured.

There's some current drift in the ELG-2 Electron Gun system. This can be explained by the deforming of the tip during heating. To get a sense of this drift the current was measured for 3 hours for different settings as can be seen in figure 4.6, this drift is in line with the report of [31] where the same setup was used. As can be seen the current stabilizes after some time: therefore all measurements are performed after the electron gun was turned on for at least 1 hour.

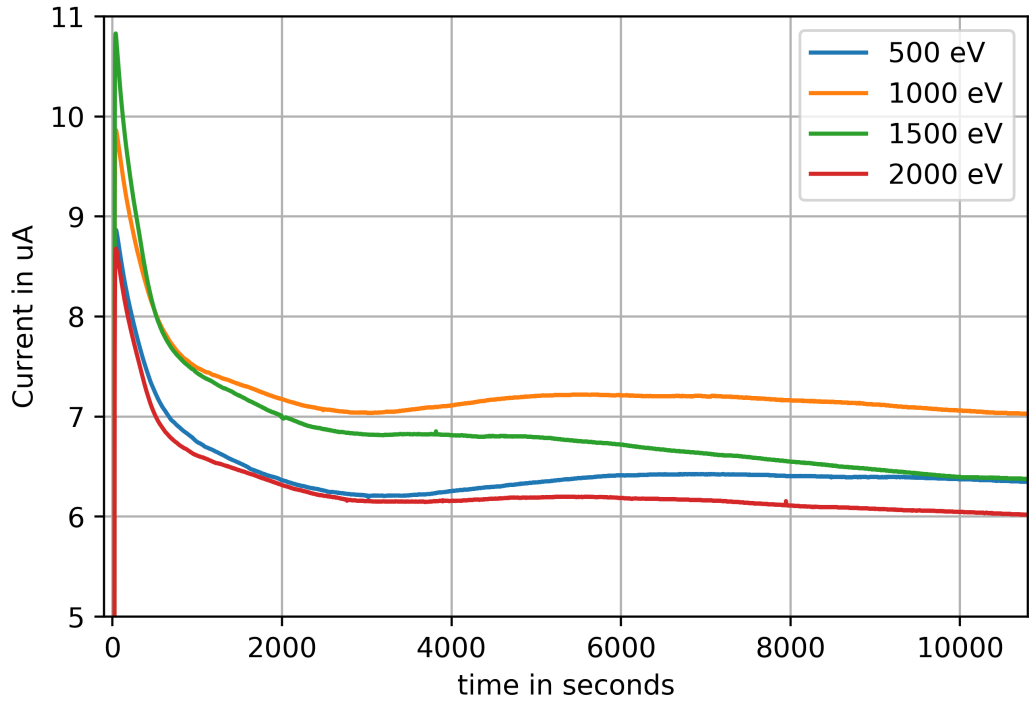

Figure 4.6: Egun current drift in time for different electron energies, measured with the Faraday cup at 200V.

But even after waiting for 1 hour there's still some drift in the current. To correct for this the following approach was taken: if the acquired image from a single electron pulse is defined as a frame. And each measurement point is a combination of settings as electron energy and pulse duration. Then for each measurement point about ~50 frames are acquired. And these ~50 frames are not taken consecutively, but with frames from other measurement points in between. The drift in the electron gun current will average out and the effect will be minimized.

4.3. Measurements using Tytest

The goal of this setup is to perform TSEY measurements on tynodes. The electron gun is used to create a pulsed electron beam and the TimePix1 chip is used as a charge sensitive detector. TSEY measurements are performed by comparing the TimePix1 response of two electron pulses: one directly on the TimePix1 chip and one on a tynode (see figure 4.7). Permanent magnets are used to deflect the electron pulse towards the correct position.

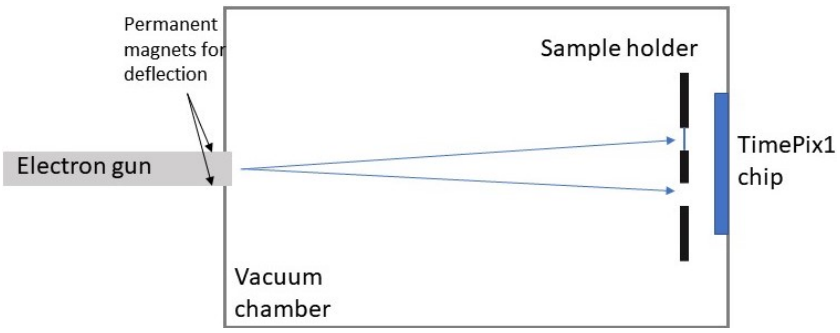

Figure 4.7: Schematic figure of the TyTest setup. Here we can see that the electron pulse is either incident on the tynode or directly on the TimePix1 chip.

The vacuum throughout the experiments was ~ 10^{-8} mbar. This figure doesn't show a 9-pin electrical feed-through that is connected to the sample holder and TimePix1 chip. This feed-through is used to bias the samples and set the polarity on the TimePix1 chip. Other instruments that are vital for the functioning of TyTest are shown in figure 4.8. The electron gun and TimePix1 chip are on opposite sides of a vacuum chamber with a transparent flange in between.

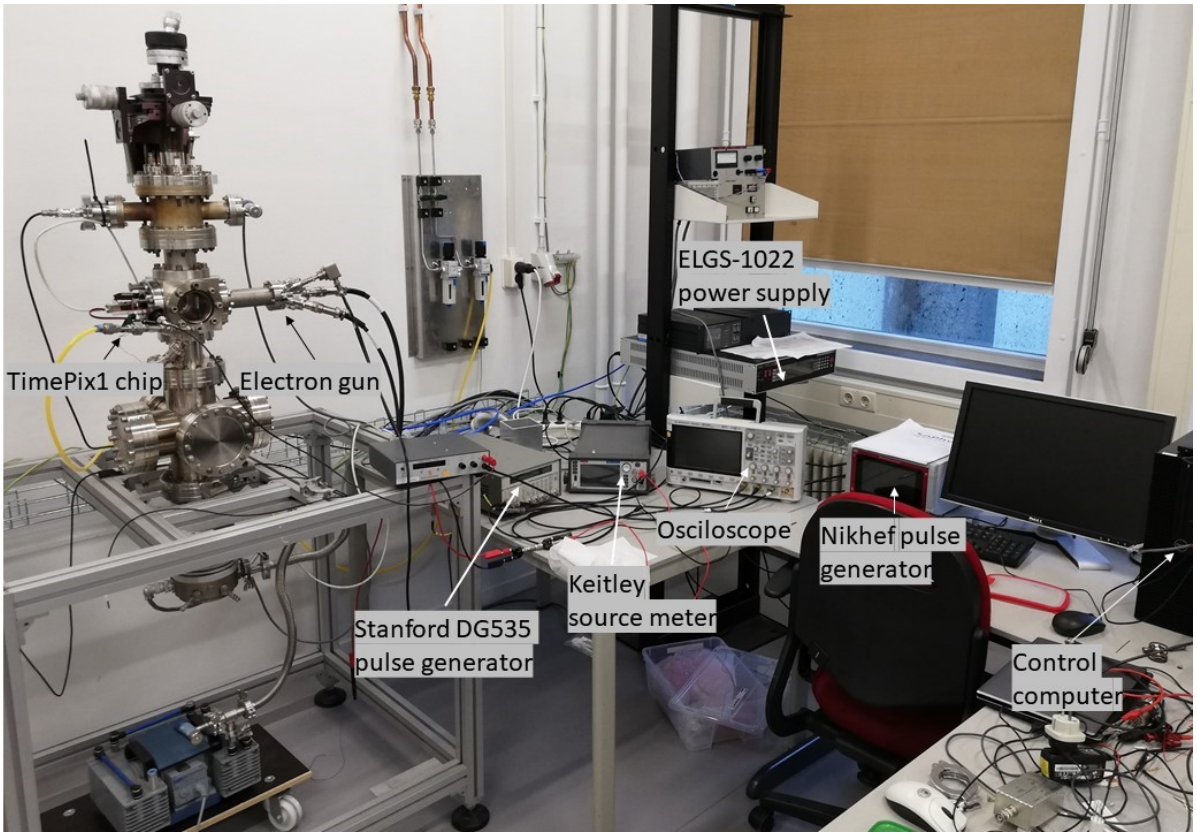

Figure 4.8: Picture of Tytest setup taken with mobile phone, all the instruments discussed are labelled.

All the instruments here are shown and labelled. As can be seen there are some knobs that can be turned on top of the setup. This gave control over the Faraday cup and a fluorescent screen inside the vacuum. By turning these knobs while looking through the transparent flange it's possible to rotate and translate them in or outside the electron beam. The fluorescent screen was used to check if the electron beam was focussed in DC mode. The Faraday cup was used to measure the electron gun current.

4.3.1. Keitley 2450 source meter

The Keitley 2450 source meter is used to perform current measurements while keeping samples on a certain potential. This was useful when measuring the current from the electron gun with the Faraday cup (see figure 4.6). Another task was to force a negative voltage on the tynode in order to create a electric field between the TimePix1 chip and the tynode. By applying the voltage this way the current going to the tynode can be measured and limited. The source meter receives instructions on which voltage to set on the tynode from python.

4.3.2. Nikhef pulse generator

This pulse generator is able to make pulses up to 60 V, with a pulse width range between 20 ns and 100 µs. From 20 ns to 990 ns in steps of 10 ns, and from 1 µs to 100 µs in steps of 1 µs. The rise and fall time are ≤ 1.6 ns and ≤ 1.4 ns respectively for a 60 V pulse from 10 % to 90 % [32]. This device was made by Hans Verkooijen at Nikhef in Amsterdam and is not commercially available. It was used to create the electron pulses from the electron gun system. As explained above, a grid voltage is applied which doesn't allow the electrons to escape the cathode. By using this pulse generator to sent pulses to the electron gun grid, it allows electrons to escape

for a short period of time. This creates the electron pulses that are used in this report.

4.3.3. Stanford DG535 Pulse generator

A practical problem with the TimePix1 chip is that the software used to communicate with the TimePix1 chip had no option to be commanded by a programming language. Also the signals sent by the computer to start or stop a measurement were not fast and accurate enough to coordinate with the electron pulse. Therefore a workaround was made using the Stanford DG535 Pulse generator. The TimePix1 chip was used in "external mode", which meant external trigger signals, generated by the Stanford DG535 Pulse generator, would determine when the shutter was open. By controlling the input trigger of this pulse generator the TimePix1 chip could be controlled using Python.

4.3.4. Oscilloscope DSO-X 3054A

The oscilloscope was used as the master trigger of the system as it triggered both pulse generators. Using Python a command was sent to the oscilloscope to give a trigger signal, which made it possible to automate all measurements. During the measurements the oscilloscope was used to check whether the busy signal of the TimePix chip was correctly aligned with the shutter close signal.

4.3.5. Control of Tytest

All these instruments work together to perform the measurements. The computer makes sure that all the instruments have the correct settings. A block diagram of how this is achieved can be seen in figure 4.9. After all the settings are changed to the correct values, the computer gives the trigger command to the oscilloscope. The oscilloscope triggers both pulse generators which at their turn put the shutter open on the TimePix1 chip and sent a 30-40 V pulse to the electron gun system causing a electron pulse to be emitted. After a fixed time the shutter of the TimePix1 chip closes and SoPhy starts to readout the pixel chip. This means each time the oscilloscope received a trigger command eventually a single frame was saved on the computer. During the readout time the computer sets new setting for the next measurement.

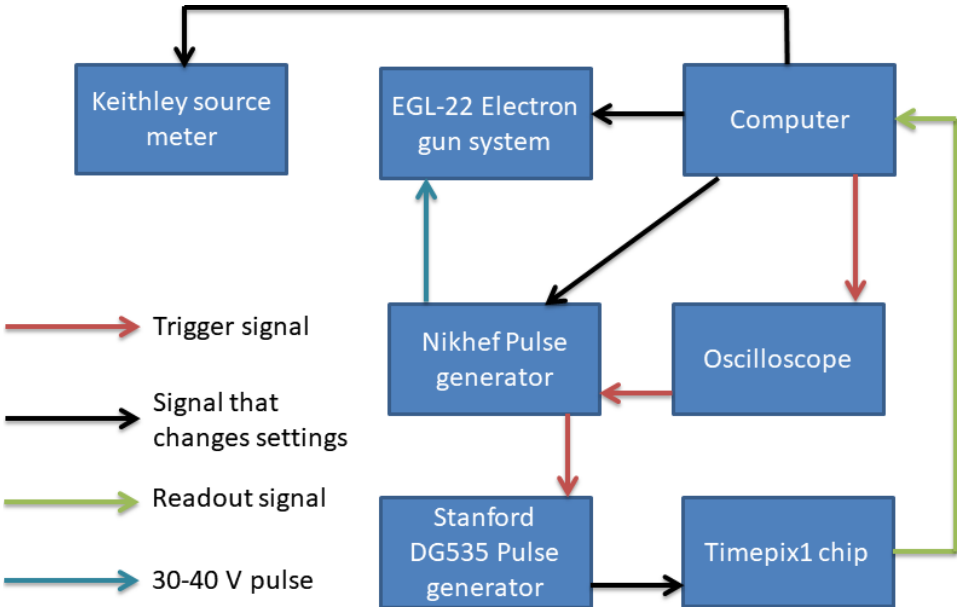

Figure 4.9: Block diagram of how the different instruments work together when performing measurements.

Most common changes were made in tynode voltage, pulse width, pulse height, electron energy and electron grid voltage. But a lot of other changes were allowed by the system. Between measurements a wait period of 300 ms was inserted to make sure SoPhy was done reading out the TimePix1 chip. If the electron gun energy was changed a additional waiting period of 60 seconds was used to let the electron gun system settle. After the waiting periods the trigger command was sent to the oscilloscope again and the process repeats itself.

A problem with Tytest is that the electron spot on the TimePix1 chip seems to vibrate in time. If a measurement with the exact same settings is repeated multiple time, a similar spot will be visible each time but

with a few pixels displacement. Investigations into the cause of these vibrations didn't amount to a suitable explanation. Therefore it was needed to average each measurement point over multiple frames, usually 30 to 50. Here also rises the importance of being able to control all relevant instruments with a programming language, because taking a lot of frames is only feasible if the frame acquisition is automated.

5
Results

In this chapter the results of the TSEY measurements will be discussed. In order to perform these measurements the TimePix1 chip needs to be calibrated using a unconventional method which is described in section 5.1.1. To justify why this unconventional method was chosen we start this chapter with how a calibration is normally performed and why this isn't a option for this work.

5.1. Measuring charge with the TimePix1 chip

Measuring charge with the TimePix chip is done in Time over Threshold mode (ToT). This means each pixel registers the time the voltage in that pixel is over a certain threshold, which is a measure for the charge collected by the pixel. A example of an calibration for another chip is shown in figure 5.1. This calibration is done by sending a test pulse to each pixel, and measuring their response. Each mV corresponds to ±50 electrons [28], which is why the x-axis has the unit mV instead of a unit of charge.

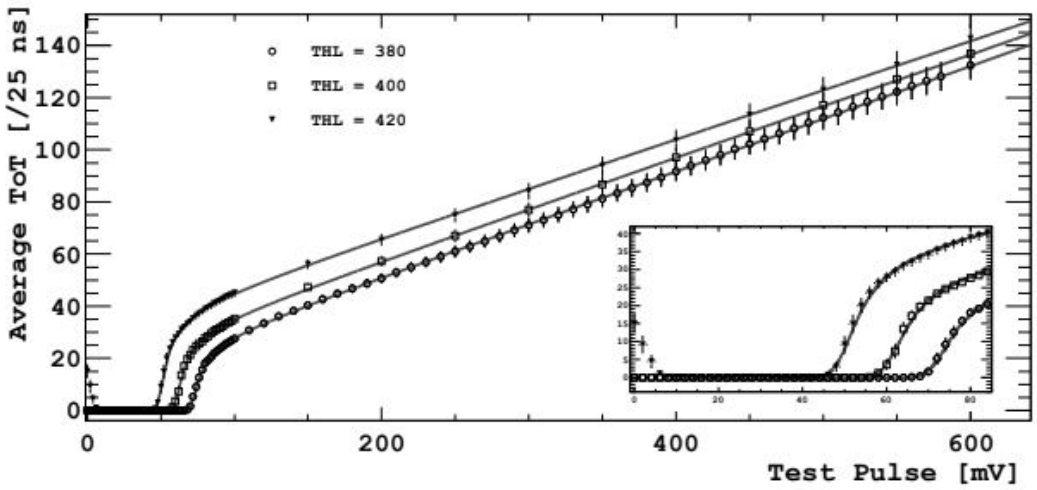

Figure 5.1: Example of a TimePix calibration, image from [27]. The three different THL values represent three different threshold values. These values cannot be used in this study. The clock speed of this measurement was 40 MHz, so each ToT unit corresponds to 25 ns.

For our chip a conventional calibration with test pulses is not feasible. The instruments that are normally used for such a calibration are adapted to work with the newer generations of the TimePix chip. Therefore we have to find a workaround in order to perform a calibration of our TimePix1 chip. In figure 5.1 we can already see that the ToT and charge don't have a linear dependence. Since the goal is to perform measurements with as little electrons as possible the non-linear region is very important. It isn't possible to add all the ToT values

in one image an convert it to a charge. This needs to be done separately for each pixel and therefore we need to calibrate the single pixel response for our chip.

5.1.1. Calibration of the TimePix1 chip

To calibrate the TimePix1 chip a known amount of charge needs to be deposited in the pixel. The obvious way to do this is with the electron gun. However this gives a problem: it's not known how much charge is deposited in each pixel per electron pulse. It is possible to measure the current of the electron gun using the Faraday cup, and thus know how many electrons in total are in each pulse. But each spot consists of multiple pixels as is shown in figure 5.2 and the distribution of charge within the spot isn't known. Normally this is a Gaussian distribution, but in this setup that assumption cannot be made for multiple reasons. First the cathode of the electron gun is very old and doesn't have a uniform electron emission [31]. Second the TimePix1 chip is not placed at the working distance of the electron gun, and therefore the focus is not perfect. Since the number of electrons deposited in a pixel per pulse is unknown, we make the following assumption:
The number of electrons deposited in a pixel per electron pulse scales linearly with the pulse duration of the electron pulse.
The next step is to acquire a image of a 20 ns pulse directly on the TimePix1 chip. The 20 ns was chosen because that's the minimum pulse duration possible with the TyTest setup. After the 20 ns image is acquired

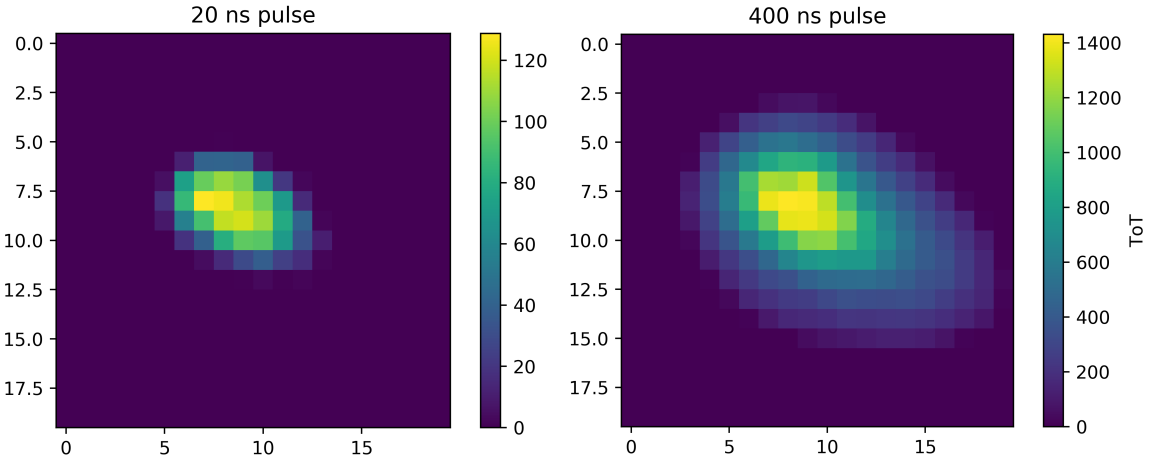

(a) 62 non-zero pixels

(b) 174 non-zero pixels

Figure 5.2: A 20 ns and a 400 ns pulse with 1400 eV electrons directly on the TimePix1 chip. A 100 MHz clock speed was used so a single ToT unit corresponds to 10 ns.

the pulse duration is increased in steps of 10 ns to 400 ns. As can be seen on the right in figure 5.2 a lot more non-zero pixels are visible in the 400 ns image. All the pixels that are zero for a 20 ns pulse, and non-zero for a 400 ns pulse cross the pixel threshold within this range. This means at some pulse duration PW_T the pixel receives just enough charge to cross the threshold. Later on this PW_T is used to characterize the single pixel responses. For now it's important to know that a single pixel response is acquired for a group of pixels by looping once through the pulse durations.

If the ToT values of a single pixel are plotted versus the pulse duration of the electron pulse, a curve as in figure 5.1 should be obtained with on the x-axis the pulse duration instead of the test pulse height. This is shown in figure 5.3, but the x-axis in this graph has units that are a bit unusual. Just as figure 5.1 uses Volts as a linear measure of charge (1 mV = ~50 electrons), we use pulse duration (without knowing the conversion yet). The pulse duration represents a certain amount of charge collected on a pixel. Later on this will be changed to a actual unit of charge, but for know this is not yet possible.

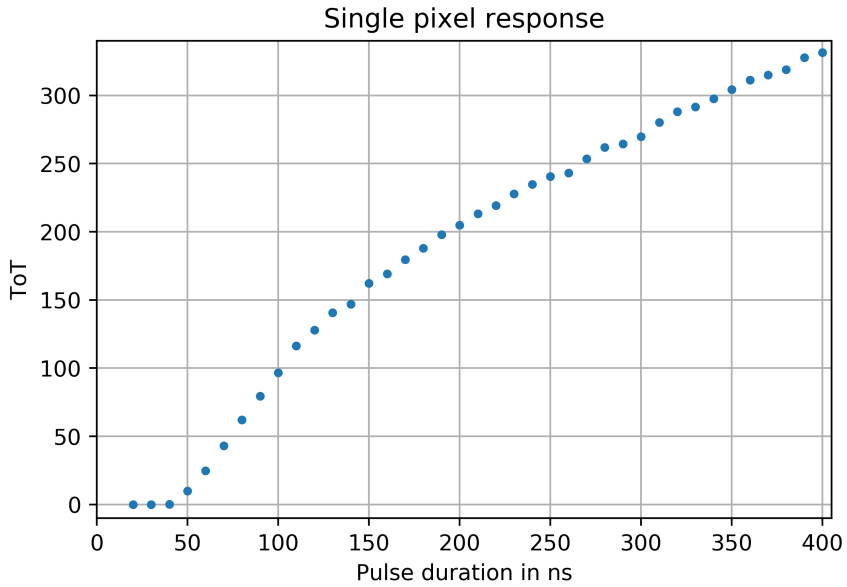

Figure 5.3: Single pixel response for a beam energy was 1400 eV, each measurement point is averaged over 300 points. The pulse duration started at 20 ns and is increased in steps of 10 ns to 400 ns. This measurement was performed using the 100 MHz clock speed.

In this figure the non-linear part of the curve is clearly visible. The ToT value is zero for 20, 30 and 40 ns pulses and begins to rise at the 50 ns pulse. This means PW_T will be between the 40 and 50 ns. As the pulse duration is increased we see that more charge is collected on the pixel and thus the ToT rises. Note a similar graph is obtained for all non-zero pixels in figure 5.2. If we want to compare the single pixel responses for multiple pixels, we need a consistent way of characterizing these graphs. First the x-axis is converted to charge, the unit that will be used at first is Multiple of Threshold (MoT), where one MoT is the threshold of a pixel. Later this unit will be related to a certain number of electrons. The following assumption is made:
If the equalization is done correctly all pixels have the same threshold value in terms of charge
So, one MoT in pixel 1 is the same amount of charge as one MoT in pixel 2. This is only true within the margin of $THS/15$ as explained in section 4.1.2. To convert the x-axis a point is needed where the charge in a pixel can be related to the pulse duration. This point is called the PW_T and here the ToT starts to rise, because here the charge collected in the pixel is one MoT. The x-axis is transformed by dividing each pulse duration by PW_T. By transforming the x-axis the single pixel responses are now in units of charge instead of pulse duration. In figure 5.4 the conversion is illustrated.

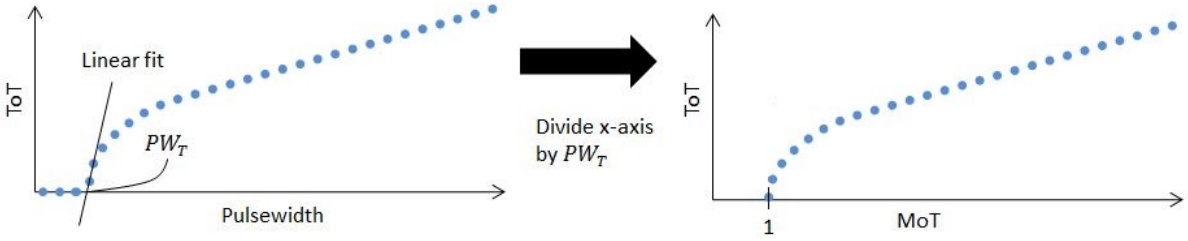

Figure 5.4: Illustration of how the x-axis conversion from pulse width to MoT is done.

The pulse duration PW_T is found using a linear fit through the first two measurement points where the ToT > 0. This graph on the right should look the same for all pixels. Note that this is not a shift in the x-axis but a division. Since the spot doesn't have a uniform electron distribution, not all pixels will have the same PW_T. Therefore single pixel responses that have a higher PW_T value will extend to less MoT. Using this method it's possible to calibrate a single pixel. The following settings were used:

- Clock speed of TimePix1 chip: 100 MHz
- pulse duration varied from 20 to 400 ns in steps of 10 ns
- 300 frames per pulse duration
- pulse height of pulse generator: 40V

- Electron gun grid: -40V
- Electron gun energy: 1400 eV
- Electron gun focus: 550V
- Electron gun source: 1.4V
- Electron gun anode: 205V

It's not feasible to calibrate each pixel separately (262144 pixels), therefore a calibration of multiple pixels will be averaged to obtain a representative single pixel calibration. Note that the spot size of a single pulse with electrons spans multiple pixels. For this calibration 174 pixels were non-zero for the maximum pulse duration of 400 ns. Only pixels where 10 ns < PW_T < 40 ns holds are taken into account. For pixels where PW_T < 10 ns no accurate estimation can be done because the amount of charge received is always far above threshold. These ~20 pixels are in the center of the 20 ns pulse in figure 5.2. The upper limit of 40 ns is a bit arbitrary and was chosen so each single pixel response will extend to at least 10 MoT (highest pulse duration was 400 ns). This way another ~80 pixels are deemed not suitable for this calibration. These pixels are on the outer regions of the 400 ns pulse in figure 5.2. The calibration continues with the single pixel responses of the 76 pixels that are left. These results are shown in figure 5.5 where we each thin line represents a single pixel. The thicker blue line is the fit that is done trough all be measurement points which will be discussed later. Here we see the single pixel calibrations for 76 pixels in total, and the spread is quite big. A possible

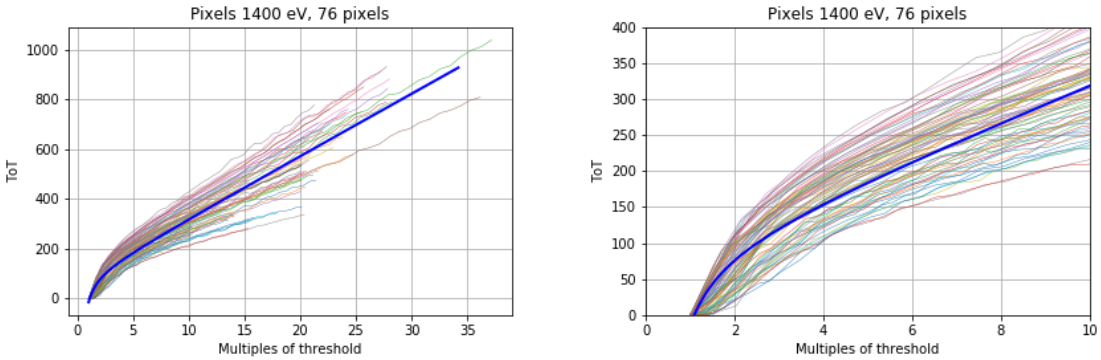

Figure 5.5: Left: full calibration curve. Right: non linear part of calibration curve.

explanation for this is that the assumption for similar thresholds is not accurate enough. Per chip there are only 16 possible thresholds according to equation 4.1. With a THS value of 80 the step size in the threshold is ~ 125 electrons, which could be too much. Another possibility is that the variation in gain of the pre-amplifier differs between pixels, although this is not seen in other TimePix1 chips. To verify if this calibration is done correctly its useful to check if the slope of a single pixel response is dependent on its position. Therefore a linear fit is done through the last three measurement points for each pixel. The slope of this fit is shown in figure 5.6 on the left. On the right of this figure the estimated PW_T of all pixels is shown.

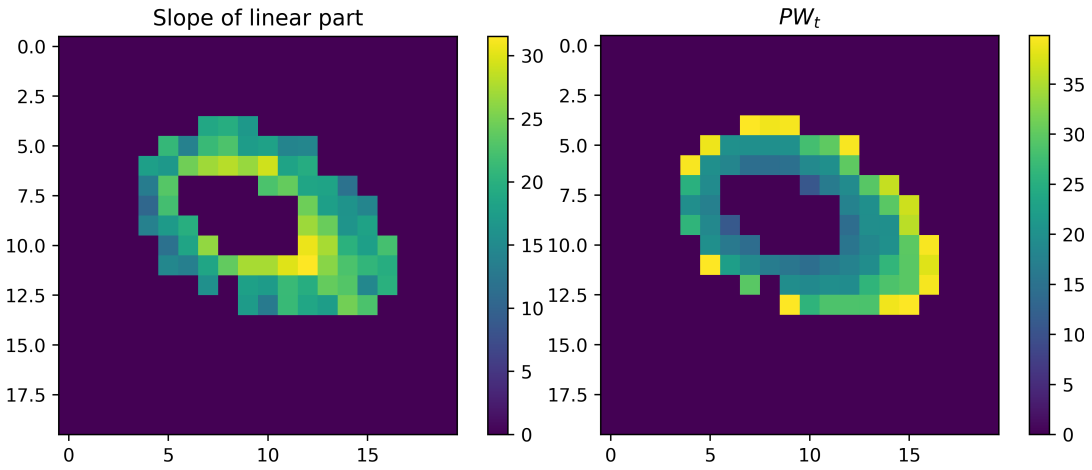

Figure 5.6: Left: This figure represents the slope of the linear part in the single pixel response. The unit of colorbar is ToT/MoT. Right: This figure represents the estimated PW_T for each pixel. The unit of the colorbar is ns. The hole in the middle are pixels that are neglected in this calibration because $PW_T < 10$ ns.

The slope of the linear part is expected to have a random distribution. Unfortunately we see that pixels close to the center tend to have a higher slope. A possible explanation could be that the PW_T values are estimated inaccurately. This could lead to relatively big variations in the slopes of the single pixel responses, because the PW_T values are used to transform the x-axis. To check if this is the case the estimated PW_T values are shown in figure 5.6 on the right. Here we see that the PW_T values behave as expected. Pixels far from the center will cross the threshold at an higher PW_T. However this does not rule out that the PW_T values are estimated inaccurately.

Even though the single pixel calibrations do not behave as similar as we had hoped for, we still continue using this result to try and see if it's possible to do TSEY measurements on membranes. The behaviour of the averaged single pixel response can be described using a surrogate function [33] [31] [27]

$$f(x) = ax + b - \frac{c}{x-d} \tag{5.1}$$

where x is used as a measure for charge in MoT and the constants a, b, c, d determine the shape of the curve. The results of this fit are: $a = 24.9 \pm 0.3 \ \frac{\text{ToT}}{\text{MoT}}$, $b = 78.8 \pm 5.8$ ToT, $c = 96.1 \pm 23$ ToT $\cdot$ MoT and $d = 0.2 \pm 0.2$ MoT. The uncertainties are one standard deviation given by the fit function. It's unfortunate that the constants c and d, which have great influence on the shape of the non-linear part, have such high relative uncertainties. When the goal of this calibration was to accurately describe the non-linear part of the single pixel response. Looking at equation 5.1 it's possible to see that the slope of the linear part is given by the constant a, which according to the fit $a = 24.9 \pm 0.3 \ \frac{\text{ToT}}{\text{MoT}}$. Since ToT is a unit of time and MoT is a unit of charge, a has the unit of an inverse current. This current physically represents the drain of the TimePix1 pixels. Therefore it's possible to use this to associate a certain amount of charge to the unit MoT. The drain was set for 0.393 ± 0.06 nA [28] for this calibration, which corresponds to $2.4 \pm 0.4 \frac{\text{electrons}}{\text{ns}}$. To rewrite the inverse of a the clock speed of the TimePix1 is used (100 MHz), which means 1 count represents 10 ns. For a^{-1} this becomes

$$a^{-1} = \frac{1}{25}\frac{\text{MoT}}{\text{ToT}} = \frac{1}{25 \cdot 10}\frac{\text{MoT}}{\text{ns}} \tag{5.2}$$

which should be equal to the drain. This leads to a MoT of 1220 ± 150 electrons, which sets the threshold at the same amount of charge. The uncertainty in this number is substantial because not only there's a uncertainty in the constant a, there's also a uncertainty in the drain current of the pixel. The found MoT value is comparable to the THR values used in [27] of ~ 1020 electrons for a similar threshold setting. This could also explain the variation in figure 5.5, since a step size in THR of ~ 125 electrons is a relative big number if the average THR value represents 1220 electrons. Nevertheless we will use this calibration data to do TSEY measurements on a thin membrane.

5.2. Transmission yield measurements

The goal was to do TSEY measurements on multiple samples but due to time constrains only measurements on one sample are performed. A schematic image of the sample is shown in figure 5.7 where we see the

sample structure. The Alumina layers are the membranes that should multiply the electrons.

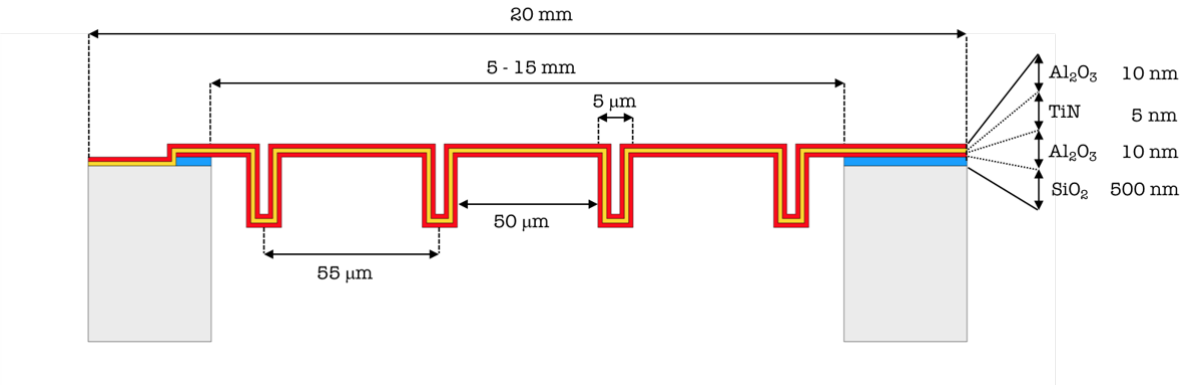

Figure 5.7: Schematic image of sample (not to scale). Image and sample provided by Hong Wah Chan.

The conductive 5 nm TiN layer is sandwiched in between to prevent charge up. Later batches will only have a conductive layer on the incident side of the tynodes. The area was 5 mm by 5 mm and the sample has a octagonal structure as shown in figure 5.8. The structure increases the mechanical strength of the membrane, as well as simulates the behaviour of curved tynodes.

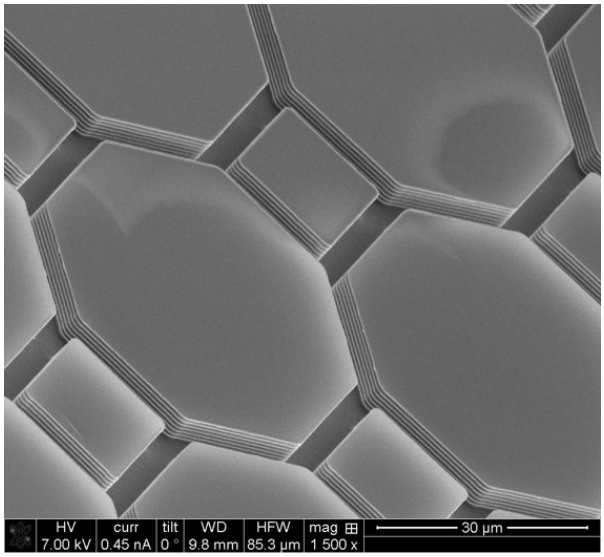

Figure 5.8: SEM image of tynode, courtesy of Hong Wah Chan.

Because the "vertical walls" in this membrane are only 25 nm thick, the assumption is made that this tynode has a active area of 100 %. The measurement was set up as follows:

- Energy from 1350 eV to 1800 eV in steps of 50 eV
- pulse duration varied from 220 to 300 ns in steps of 20 ns
- potential of tynode varied from -100 V to -200 V in steps of 25 V.
- an average over 50 frames was taken for each combination of these settings

Using these settings the electron gun was aimed directly at a blank TimePix1 chip, and a measurement is performed for each combination of pulse duration and energy. The copper input pads of the TimePix1 chip have a RSEY curve which is measured in [31]. The obtained results are corrected for the RSEY curve to obtain a MoT value for each combination of pulse duration and energy. After this was done the electron pulse was deflected towards the tynode, and a MoT value was obtained for each combination of: tynode potential, pulse duration and electron energy. The tynode measurements are not corrected for the RSEY of the copper input pads, because the negative potential applied on the tynode will push back all secondary electrons. The TSEY value is the tynode MoT value divided by the blank TimePix1 chip MoT value.

Another effect of this negative tynode potential is that the incident electrons will be slowed down. Therefore the transmission yield will be shown as a function of landing energy. The spacing between the tynode and the pixel chip is ~ 1.5 mm, which puts the electric field between $6.7 \cdot 10^4$ to $13.4 \cdot 10^4 \frac{\text{v}}{\text{m}}$ for a potential difference from -100 to -200 Volts. The defocussing due to this potential is not taken into account in this research. Unfortunately the spot size increased for higher energies. At 1800 eV the spot size was bigger than the active area of the tynode (5 mm by 5 mm). Therefore energies higher than 1800 eV are not taken into account. In figure 5.9 the TSEY for a 300 ns pulse is shown for three different tynode potentials. The results for all other pulse durations with all the tynode potentials are shown in appendix B.

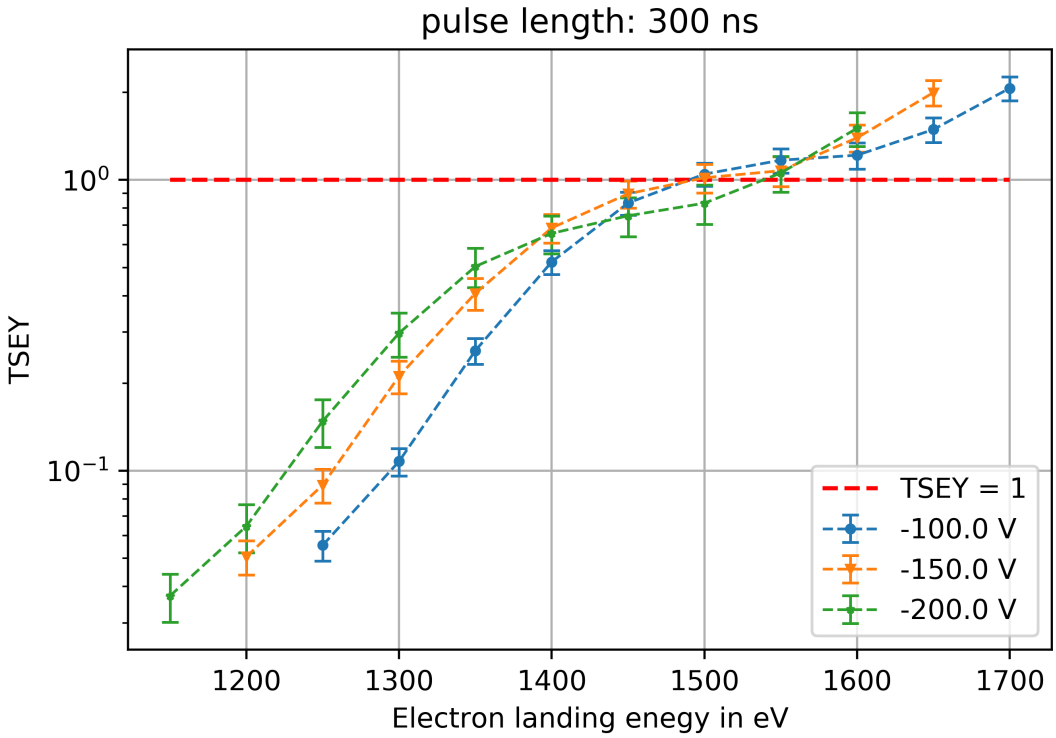

Figure 5.9: TSEY measurement for a 300 ns pulse and three different tynode potentials. The uncertainties are one standard deviation.

Around a landing energy of 1500 eV the TSEY exceeds one, which means there's electron multiplication. It's unfortunate that it's only possible to measure up to a electron energy of 1800 eV, because the peak in TSEY seems to be at higher energies (at 2500 ev for a 25nm membrane in [6]). The measurements shown in this graph do not agree with each other: the TSEY seems to be different at lower landing energies, after 1400 eV the measurement points do agree more but are still not within the uncertainty. For energies below 1400 eV there seems to be a dependence on the tynode voltage. A possible explanation could be that due to a stronger electric field between the TimePix1 chip and the tynode, the transmitted secondary electrons are spread out over less pixels. This makes it more likely for a pixel to cross the threshold. Another possibility is that the copper pixel pads have a different RSEY for 100 and 200 eV electrons. However due to the negative tynode potential emitted SE's from the copper pads should be pushed back in the material. Only when the SE's shift to adjacent pixels this would blur out the spot. In figure 5.10 the results are shown for different pulse durations at a single tynode potential. The results of all other combinations of tynode potentials and pulse duration are shown in appendix B.

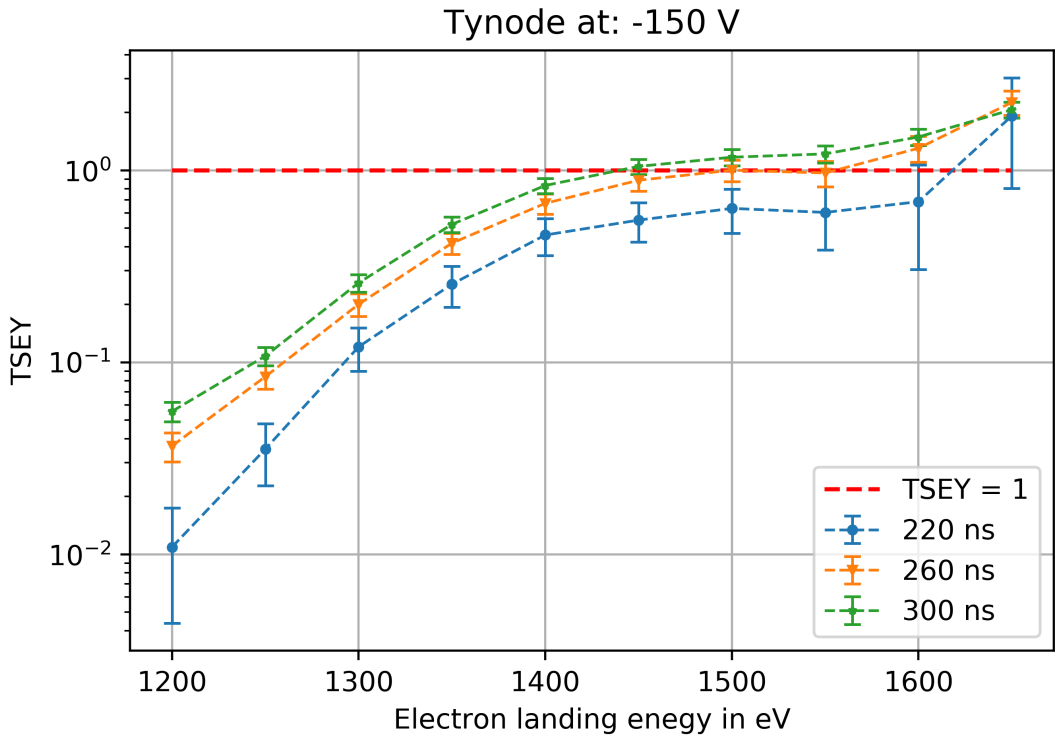

Figure 5.10: TSEY measurement for a -150 V tynode potential and three different pulse durations. The uncertainties are one standard deviation.

Here a clear unexpected influence of the pulse duration on the TSEY is observed. This could be explained by more pixels crossing the threshold for longer pulse durations. This would mean that for short pulse durations more pixels don't receive enough charge to cross the threshold. If this is the case it seems likely that also for a 300 ns pulse duration charge is not being taken into account.

Another observation is that the error bars are bigger for short pulse durations. A possible explanation is the following: The non linear part of the calibration had a high uncertainty. Therefore pixels that receive a relatively low amount of charge will have a bigger uncertainty. On average we would expect that pixels receive less charge for a shorter pulse duration. Which could explain why the error bars of the 220 ns pulse are bigger compared to the other pulses. This reasoning would agree with the explanation from before that not all pixels cross the threshold.

One would expect that a tynode emits the secondary electrons more or less on the same place where the electron pulse is incident. To compare how much the electrons emitted from the tynode are spread out a comparison is made in figure 5.11.

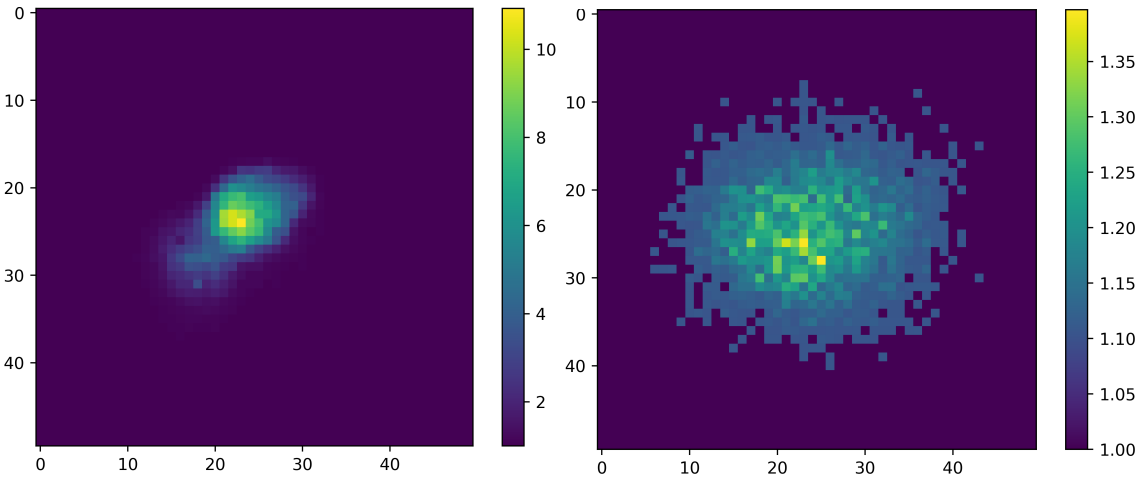

(a) Spot directly on pixel chip, total charge is 1524.9 MoT.

(b) Spot created by electron pulse on tynode, total charge is 796.1 MoT.

Figure 5.11: Comparison of the spot shape between a beam directly on the Pixel chip, and a beam on the tynode. A 300 ns pulse at 1500 eV with a tynode potential of -100 V.

Here it can be clearly seen that there's a huge spread in where the electrons arrive at the pixel chip. Another interesting observation is that there's 10 MoT of charge deposited in a single pixel on the TimePix1 chip, but only 1.35 MoT when a tynode is placed in front of the beam. It could be that during the emission from the tynode there's some coulomb interaction between the electrons which cause them to spread out. Another possibility is that the tynode potential causes the pulse to spread before the electrons arrive at the tynode. This figure does suggest that a lot of electrons emitted by the tynode aren't measured by the pixel chip. The edge of figure 5.11b has MoT values close to one, which is the minimum amount needed to cross the threshold. There's likely also charge being absorbed by the pixels next to the edge, but not enough to cross the threshold. This does confirm the possible explanation on why in figure 5.10 there's TSEY dependence on pulse duration.

6

Tynode stacking at Nikhef

In order to produce a prototype of the Tipsy detector a method needs to be found to create a aligned stack of tynodes. A ZEISS Axio-zoom V16 light microscope in combination with two µm precision manipulators placed in a clean room at Nikhef in Amsterdam were used for this task. The stacks were aligned using a self align mechanism that will be discussed first. After this the microscope and how it's used to confirm the alignment will be explained. Finally the manipulators and their advantages will be discussed.

6.1. Building a stack

An image of a tynode can be seen in figure 6.1 on the left. The first thing that stands out are the straight lines on the sides that go on to the edge at one side. These lines are grooves that act as a self alignment mechanism. By placing a 200 µm diameter glass wire in these grooves the domes of the stacked tynodes should align if the distance from the domes to the grooves is the same. This is an assumption and to check this the displacement between the different tynodes is measured. These grooves extend to the edge of the tynode so the glass wires can stick out of the stack. This is useful for checking if the wires are still in place when the stack is completed.

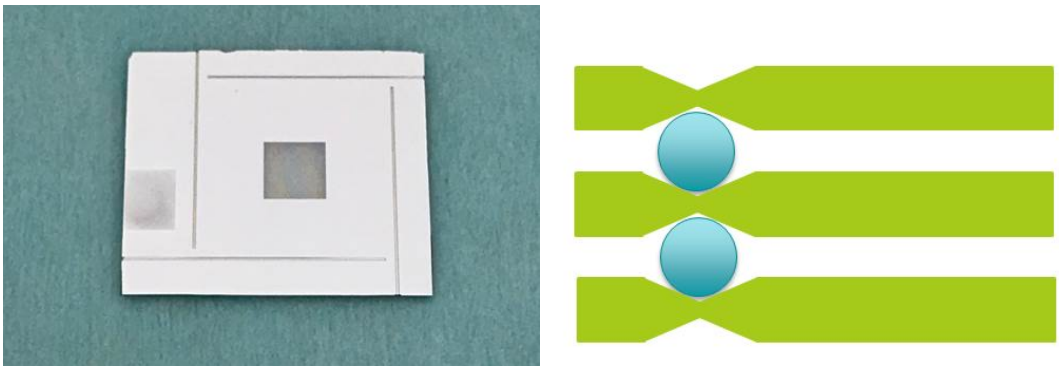

Figure 6.1: Left: picture of tynode (taken with phone camera, not the microscope). Tynode's provided at courtesy of Violeta Prodanovic [6]. Right: Schematic drawing of self alignment mechanism.

Another thing that stands out when looking at the tynode is the small square on the left side. This is the place where a high voltage can be applied. The active area which contains the domes is the square in the middle. In this area an array of 64 by 64 domes is fabricated. Note these are not the same tynodes as used in the measurements with tytest! The first step is placing a glass rod aligned with a groove between the active area and the groove. Using tweezers this rod can be rolled inside the groove. When a rod is placed in all four grooves the next tynode is placed on top. By moving the upper tynode around until it settles in place a stack is created. This was first done using dummy tynodes without a active area, see figure 6.2. Note these tynodes were stacked by hand.

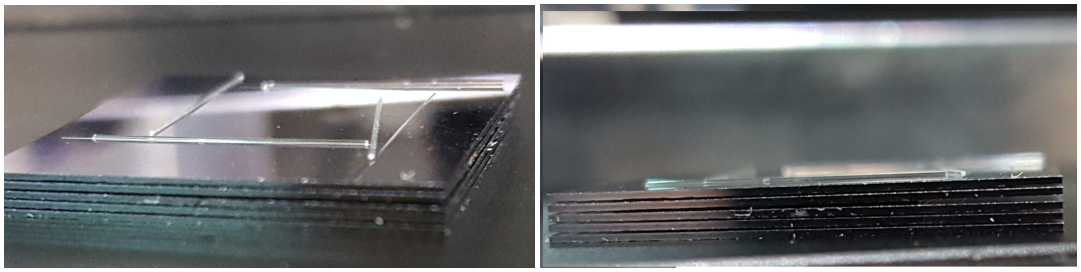

Figure 6.2: Left: dummy tynode stack with focussed on the grooves, right: dummy tynode stack focussed on the edge.

Here the first stack of tynodes can be seen. The first thing to note is that the glass wires don't extend beyond the edge of the tynode as shown in figure 6.1. The reason is that these are dummy tynodes, the real tynodes will have grooves that extend to the edge. Between second and third tynode (counting from the top) a increased spacing can be seen on the right side of the stack. This means the glass wire is not fully in the groove and this stack has failed.

6.2. Zeiss microscope

A ZEISS Axio-zoom V16 light microscope was used to image all parts of a tynode and check for any irregularities or manufacturing errors. An picture is shown in figure 6.3. The microscope is able to focus on a certain height with µm precision. Therefore it's possible to measure height differences, as long as the focus is defined properly. Another feature of this microscope is its ability to look trough holes with a diameter in the order of 10 µm. This made it possible to look trough hole in a tynode and see the tynode underneath. This did greatly reduced the resolution.

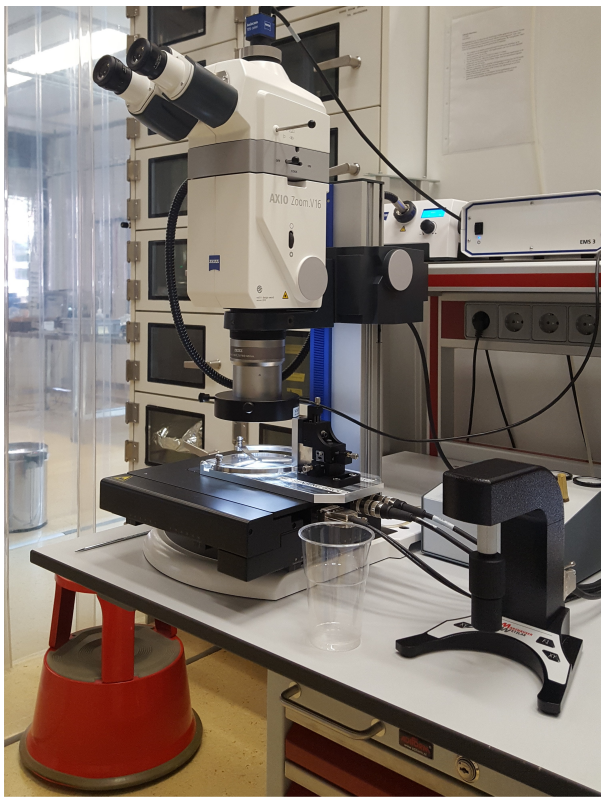

Figure 6.3: Photograph of Zeiss microscope.

The microscope was used in combination with the software ZEN 2. This gave very useful options such as live imaging, auto focus, dynamic focus and height measurements.

6.3. Manipulators

The are two manipulators shown in figure 6.4. The first one is provided at the courtesy of the "THZ Sensing group". This manipulator controls the sample surface underneath the microscope, and is used to translate samples with respect to the optical axis. What makes this manipulator such a useful instrument is its ability to save positions with μm precision. By aligning features with the optical axis of the microscope and saving the position, distances between these features can be determined. This is useful when checking the displacement between different tynodes, but also when checking for manufacturing errors.

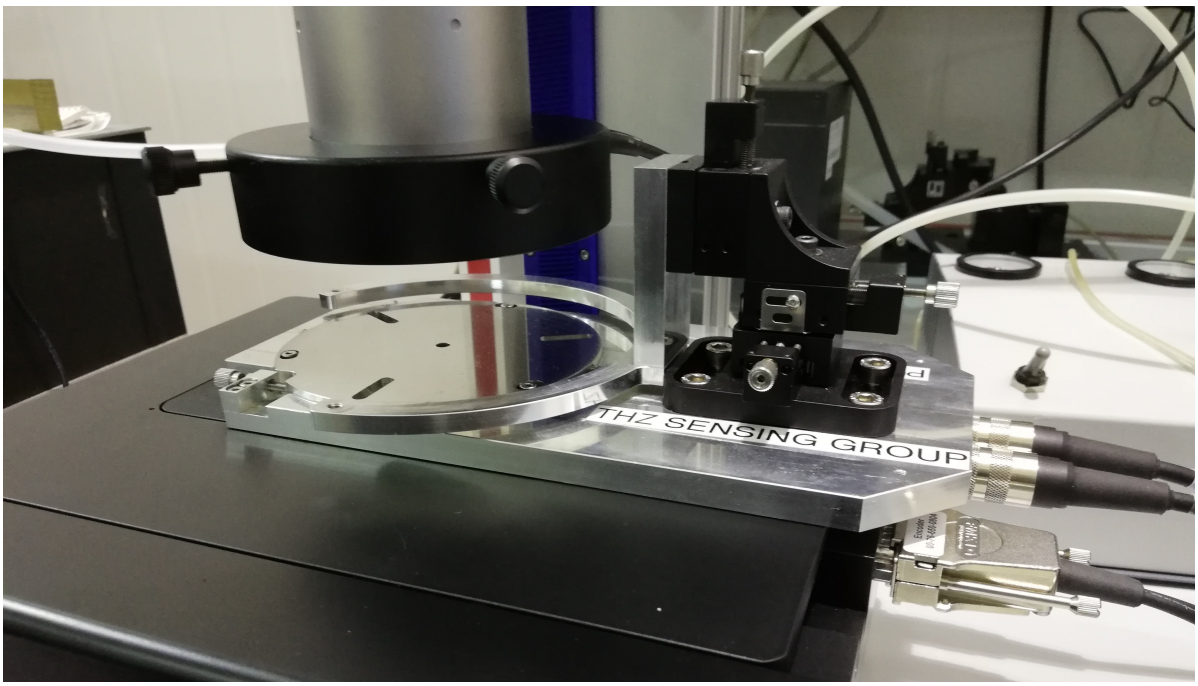

Figure 6.4: Photograph of the manipulators. Three legs are connected to a ring which can be moved separately from the surface. Due to the reflection of the light one tip isn't visible.

The second manipulator moves the metal circle by turning small screws to allow translation in three direction. In the metal circle there are three screw holes in which legs can be mounted. By glueing a tynode to these legs this manipulator allows for very accurate placement of the tynode above anything fixed on the surface below the microscope. It's not possible to retrieve a position once it's gone since the screws are turned by hand.

All these instruments in combination should allow for high resolution light imaging and measuring translations in three dimension with μm accuracy. The placement new tynodes can be controlled and imaged to ensure accurate positioning of the tynodes. Using this setup a stack was made and the displacement was measured.

6.4. Alignment of Tynodes

It's a challenge to stack these tynodes without damaging them. This is very delicate work as the membranes easily break and this took some practice. The method that eventually worked had the following approach: First place the glass wire parallel to the groove in the area between the active square and the groove. Using tweezers roll the wire in the groove and apply a little pressure on it so it stays fixed. After all four wires are fixed, carefully place the next tynode on top. Apply pressure between the square spanned by the grooves (not in the active area because that will damage the tynode) until the tynode is stuck. If pressure is applied outside the square spanned by the grooves the upper tynode will tilt which will cause all the wires to get out of the grooves. When the upper tynode is fixed the alignment can be checked by looking at the glass wires under the microscope. If all the wires stick out perfectly parallel to each other, they are fixed in the grooves correctly. This can be seen in figure 6.5 where a image of the first tynode stack is shown.

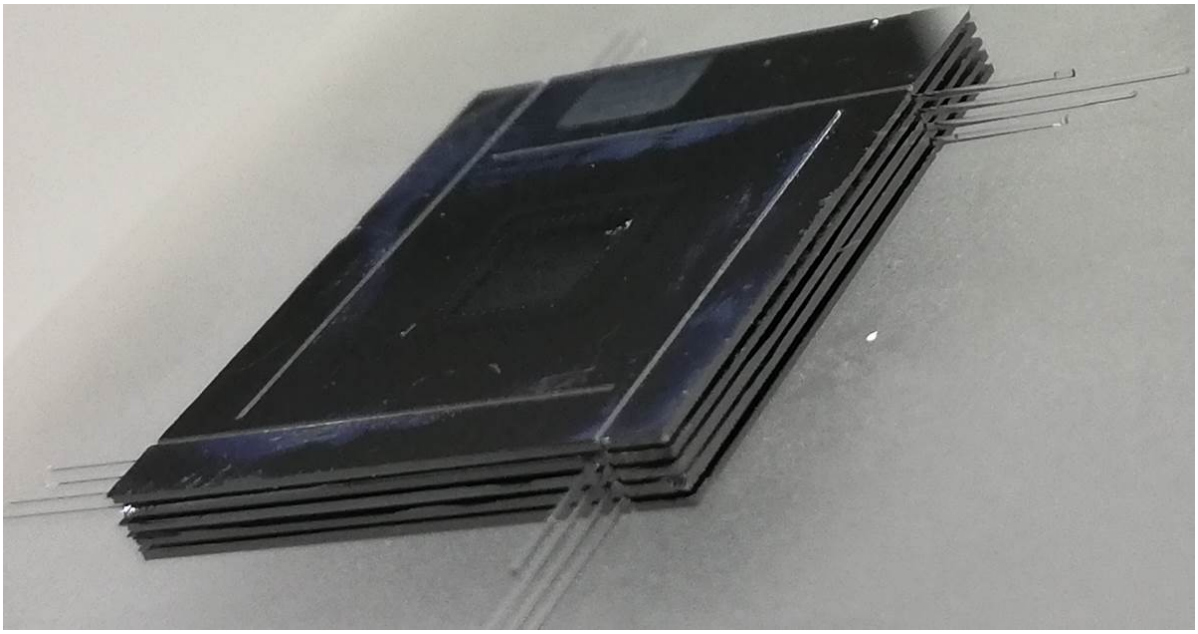

Figure 6.5: Final stack of 5 tynodes, picture taken with phone camera.

The active area in the middle of one tynode consists of 64 by 64 domes, the alignment of these domes in a stack is of interest because a displacement can cause electrons to hit the non active area of the next tynode. Some misplacement can be compensated by the focussing effect but this has a limit, for Tipsy a displacement better than 5 µm is preferred. To measure the alignment four domes are chosen, one in every corner. The chosen dome is on the 5th place diagonally (5th row and 5th column from each corner), for the bottom right corner this is shown in figure 6.6. As discussed above, feature of the Zeiss microscope is that it can show where the optical axis is located with respect to the image. By carefully aligning the optical axis with the center of a dome, the dome position can be saved. This was not straight forward because mechanical vibrations of the microscope table caused the image to shake a bit. These vibrations had an amplitude of ~ 2 µm. As can be seen if figure 6.6 the image of the upper tynode (left) is much clearer that the image of the fourth tynode (right). Therefore the uncertainty of the upper tynode is 3 µm and the uncertainty of the fourth tynode is 4 µm.

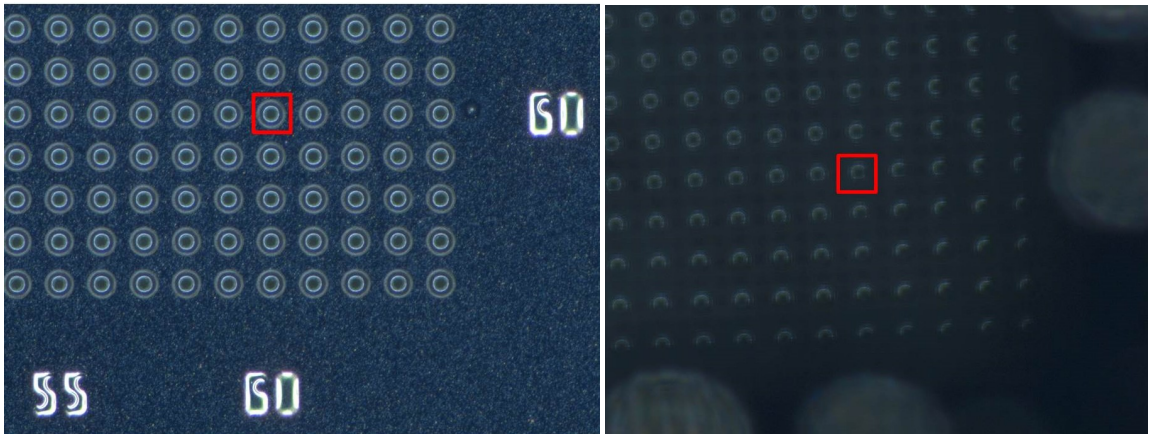

Figure 6.6: Left: microscope image of the upper (fifth) tynode. Right: fourth tynode, image obtained by looking trough the fifth tynode. The 5th diagonal dome is shown with a red square, for these domes the position was determined.

The procedure for determining the alignment started with identifying the fifth diagonal (fifth row and fifth column) dome in each corner of the upper tynode. The optical axis was aligned with the center of this dome and the position is saved. Next the focus was changed so the fourth dome is imaged. Here again the optical axis is aligned with the center and the position is saved. Unfortunately there was a constant translation

when changing the focus from the fifth to the fourth tynode. Therefore the microscope translation will be determined first. For this measurement the displacement of domes in position [row,column]: [5,5] [5,59] [59,59] and [59,5] where measured in this order (clockwise), and are referred to as dome 1 to 4. After this the whole stack was turned 90 degrees clockwise by hand and the measurement was repeated, the same for 180 and 270 degrees. This process is shown for one dome in figure 6.7. Here the measurements for a single dome are shown.

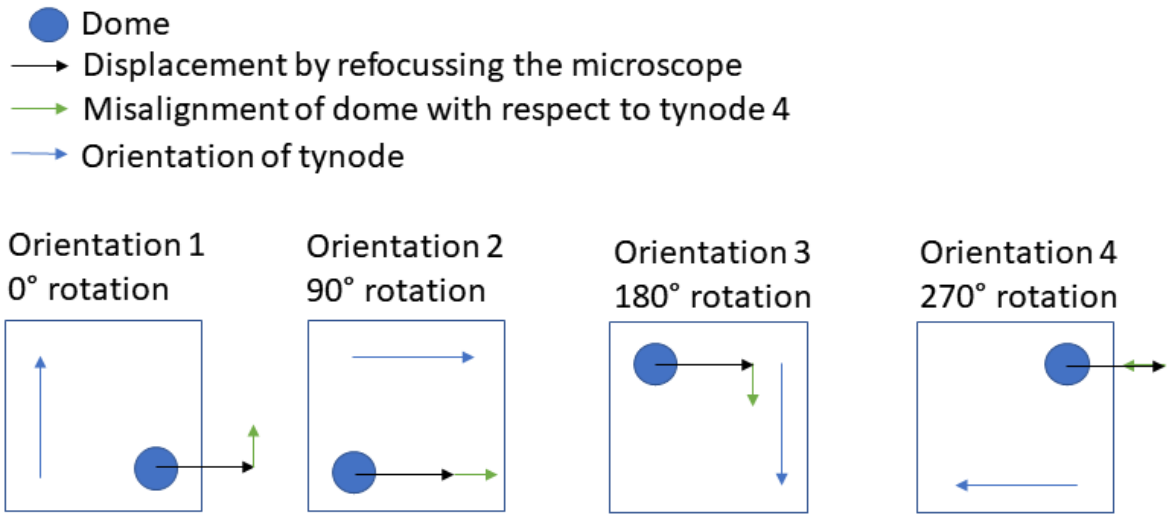

Figure 6.7: Illustration of how the measurements on the misalignment on a single dome are performed. Image not to scale.

Each measurement contains the combination of both displacements and it's not possible to distinguish them yet. In this figure it can be seen that the displacement due to the microscope should stay in the same direction after each tynode rotation. While the displacement of the dome with respect to tynode 4 rotates along with the tynode stack. This is used to distinguish the displacements. First the displacement of the microscope due to the changing of the focus was determined by adding up all displacements, this should cancel out all the displacements due to misalignment of the stack. The results are shown in table 6.1. The x and y coordinates that lead tot his result can be found in appendix C.

Dome	x displacement in µm	y displacement in µm	$\sqrt{dx^2+dy^2}$ in µm
1	10.8 ± 2.5	-6.8 ± 2.5	12.7 ± 2.5
2	7.5 ± 2.5	-5.5 ± 2.5	9.3 ± 2.5
3	10.9 ± 2.5	-6.7 ± 2.5	12.8 ± 2.5
4	10.8 ± 2.5	-6.8 ± 2.5	12.7 ± 2.5
average:	10.0 ± 1.3	-6.4 ± 1.3	11.9 ± 1.3

Table 6.1: x and y displacement of optical axis due to changing focus from fifth to fourth tynode.

From this it's possible to conclude that there is a change in position when changing the focus. This means the displacement of the optical axis due to the change in focus was 11.9±1.3 µm, which is significant since the aim for Tipsy is to have the tynodes aligned within 5 µm. By subtracting this result from the measurements the actual displacement between the 4th and 5th tynode can be found, this is shown in table 6.2.

Dome	x displacement in µm	y displacement in µm	$\sqrt{dx^2+dy^2}$ in µm
1	2.7 ± 0.9	4.7 ± 1.6	5.5 ± 1.4
2	2.2 ± 2.9	2.3 ± 1.7	3.2 ± 2.4
3	4.1 ± 1.6	2.3 ± 1.6	4.7 ± 1.7
4	2.8 ± 2.1	0.8 ± 0.8	2.9 ± 2.1
Average	3.0 ± 0.8	2.5 ± 1.7	4.1 ± 1.3

Table 6.2: Displacement of domes between the two upper tynodes.

Each measurement here is averaged over the four measurements taken under at different angles (M1 to 4). From this the displacement due to the system with glass wires is 4.1 ± 1.3 µm. This is within the 5 µm which is needed for Tipsy. One important remark to make here is that these measurements are all taken from tynode 4 and 5. To be more certain that the alignment accuracy is of this order more stacks need to be measured.

7

Conclusions and recommendations

7.1. Tytest Delft

The objective of this set up was to perform Transmission Secondary Electron Yield (TSEY) measurements on thin membranes using as little charge as possible and to demonstrate the working mechanism of the Tipsy detector. Characterization of the electron gun will using the Faraday cup showed the electron gun current peaked after turning on and dropped to 65 % of it's initial value within half an hour. After this drop the current stabilizes within ~ 5 % per hour. Therefore all measurements were done after the electron gun was turned on for at least 60 minutes. Permanent external magnets were put on both sided of the electron gun flange to create a uniform magnetic field which deflected the electrons.

A calibration of the TimePix1 chip is realized using the pulse duration of an electron pulse as a linear measure of charge. From literature a non-linearity is expected for small input charges. Since the aim is to use small amounts of charge it was necessary to accurately investigate the non-linear behaviour. A surrogate function with four variables was fitted trough the measurement points of 76 pixels. The variables that influence the non-linear part most heavily had the biggest relative uncertainties. Therefore for small amounts of charge the uncertainties were relatively large. This was probably caused by the spread in single pixel responses. The most likely explanation for this spread in single pixel responses is that the step size in threshold of ~125 electrons is too large, and the assumption that all pixels have a similar threshold is not accurate. The average threshold was found to be 1220 ±150 electrons which agrees with literature that uses similar pixel chips.

Using this calibration TSEY measurements were performed on a single tynode with a membrane of 5 mm by 5 mm. The membrane consisted out of two 10 nm alumina layers with a 5 nm conductive TiN layer sandwiched in between to prevent charging. The charge was compared for two electron pulses, one directly on the pixel chip and one on the membrane which caused the membrane to emit electrons towards the pixel chip. The TSEY is a division of those two measurements. The highest TSEY measured was 2.76 ± 0.64 for a 240 ns electron pulse at 1800 eV and a tynode potential of -125 V, which means a landing energy of 1675 eV. There were multiple unexpected phenomena observed. First and most important: if a electron pulse with a small diameter is incident on the tynode, an electron spot with a bigger diameter is observed on the other side of the tynode. Possible explanations for this effect are that there's a coulomb interaction between the electrons during the secondary electron emission by the tynode, although it seems unlikely that this would cause a spread over multiple pixels. Another possible explanation is that the electron pulse is spread out due to the tynode potential. This could mean that the size of the spot is already increases before the electrons are incident on the membrane. The cause of this effect should be investigated further before any meaning is given to the TSEY measurements. Another observation was the dependence in TSEY on the pulse duration of the electron pulse. This can be explained that for smaller pulse durations less pixels cross the threshold. And the charge deposited in those pixels aren't taken into account.

A problem with the Tytest setup is that there is a small working range in terms of electron energy in which measurements can be performed. For the TSEY measurements a relatively thick membrane was used with a

big active area. There are very thin membranes available but hey have a small active area. Those thin membranes would be more useful because the maximum TSEY value is expected to be at lower electron energies. But in Tytest there isn't sufficient control over the electron spot size to aim at these small membranes. Therefore a bigger and thicker membrane was chosen, but even for this bigger membrane only measurements up to 1800 eV could be performed. The lack of focussing capabilities also directly contradicts the aim to measure using short pulses and small amounts of charge. Even though the TimePix1 chip is very sensitive to small amounts of charges, if those charges aren't focussed not all pixels receive enough charge to cross the threshold and some charge isn't measured. Therefore a recommendation is to move the TimePix1 chip closer to the working distance, which should improve the focus capabilities. Another option would be to change the cathode of the electron gun, this should give a more uniform emission. If feasible these measurements could be performed in a more consistent matter using a pulsed SEM. This would provide imaging capabilities (HV off) to accurately know where the electrons pulse is incident while simultaneously being able to simulate the working mechanism of Tipsy by using a pulsed electron beam when the HV is on.

Another option to have better control over the electron pulses is to use a set of Helmholtz coils to deflect the electrons instead of magnets. In this research the magnets were placed by hand on the electron gun flange, this is a method that lacks reproducibility and accuracy. By using coils a more uniform magnetic field can be created which should improve the deflection capabilities.

For this project a TimePix1 chip was used because one was readily available that was mounted on a vacuum flange that can be mounted on TyTest setup. Upgrading this TimePix1 chip to a newer model, for example a TimePix3 chip, will be advantageous. First of al the response of the TimePix3 chip is more linear and can be calibrated using a setup at Nikhef. Second, properties as sensitivity, readout time, clock speed are superior. And finally the TimePix3 chip is used more frequently by others so there's more documentation available. If this is not feasible, I would not recommend to use the calibration method discussed in this report. Although it's possible to obtain a calibration this way it's inaccurate and raises a lot of questions. A better way would be to use a external probe to put a voltage on a pixel pad, and measure it's response. Another possibility could be to further investigate the test pulse function. But the best way would be to upgrade the TimePix1 chip to a newer generation TimePix chip.

7.2. Tynode stacking at Nikhef

The eventual goal of this setup is to make a stack of tynodes that could function in a prototype of the Tipsy detector. The setup is used to make and check the alignment of a stack with five tynodes. The aim is to have a misalignment which is less than 5 μm.

Stacking the tynodes is very delicate work and requires some practice and patience. Using the method described in this report it is possible to make a stack of tynodes. The combination of the ZEISS axio-zoom V16 with two manipulators is a powerful tool to investigate and stack the tynodes. Using these instruments it was possible to create a stack of 5 tynodes and measure the misalignment between the upper two tynodes. The aim is to have the tynodes aligned within 5 μm which is more than the measured misalignment of 4.1 ± 1.3 μm. It's important to note that only the misalignment between the upper two tynodes was measured, for a more complete idea of the alignment of a stack additional measurements need to be performed. In this research this wasn't an option because it would mean the only stack needed to be disassembled.

When determining the center of a dome the microscope needs to change focus between the fifth and the fourth tynode. This caused a constant translation of 11.87 ± 1.71 μm just by refocussing over a distance of ~ 200 μm. Therefore I would recommend to find out what causes this translation and maybe contact the manufacturer to see if this is a known problem.

Due to mechanical vibrations in the microscope room it was difficult to align of the center of a dome with the optical axis as the image was shaking. The amplitude of these vibrations seemed to be around 2 μm which is why the uncertainty was set on 3 μm for the upper tynode. Since the image of the fourth tynode was more fuzzy, the uncertainty is set on 4 μm. This is unfortunate because both the microscope and the manipulator used for this measurement should have sub μm precision. Therefore it would be useful to place the setup on

a vibration absorbing table, or to look for other ways to minimize these vibrations.

I would recommend to avoid glue as much as possible. In early ideas on how to hold a stack in place the idea of a vacuum glue was suggested. But when applying glue on a stack of tynodes that have to be aligned within 5 μm a soft touch with for example a brush with glue can displace everything.

8

Discussion

The unconventional method of calibration the TimePix1 raises a lot of questions. It remains unclear why pixels close to the center have a higher slope in the single pixel responses. Therefore this calibration must be used with caution which questions the TSEY results. A more accurate way would be to use a more conventional method that's already proven to work.

The electron gun didn't behave as expected. The electron spot would vibrate between measurements. The amplitude of these vibrations were clearly bigger than the pixel size which is 55 μm. Investigations to find the frequency of these vibrations or to remove them didn't amount to anything. The cause of the vibrations remains unknown.

A

Tipsy performance in time resolution

Here the preliminary results of the simulations performed by Hong Wah Chan are shown. These simulations are cited in the Chapter about Tipsy. In figure A.1 the trajectories of the electrons can be seen. An assumption made is that the TSEY of these tynodes is 3 and all TSE's are created with a energy of 3 eV emitted in a random direction normal to the exit surface.

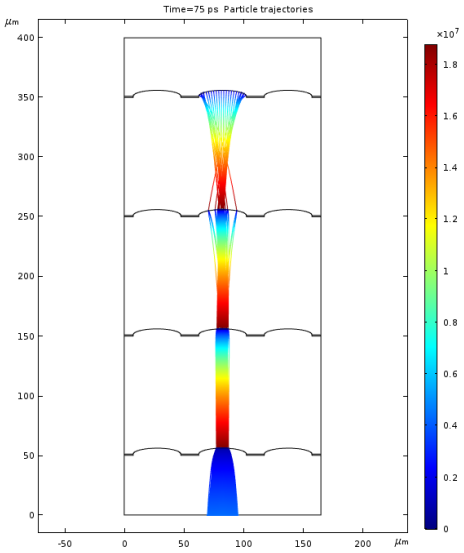

Figure A.1: Image from [16], trajectories of electrons during simulation.

The colorbar represents the speed of the electrons in m/s. Note that the highest speed corresponds with approximately 1000 eV, which means the tynodes are kept at a potential difference of 1 kV. In figure A.2 the arrival time is plotted as function of time on the left, and the derivative on the right.

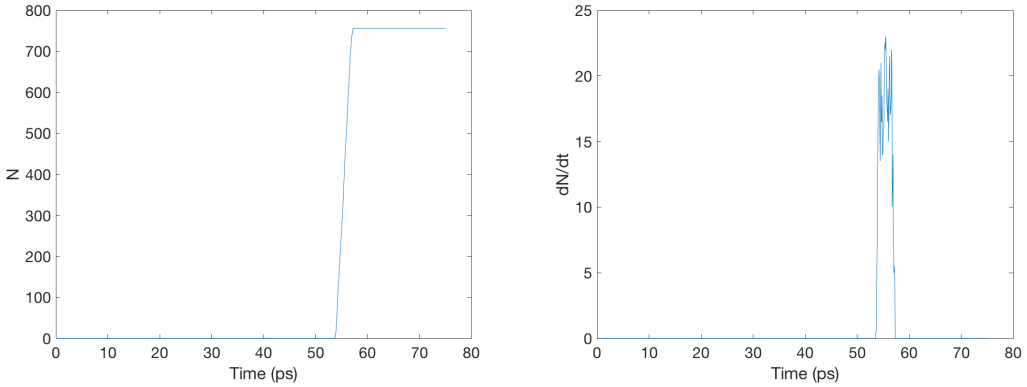

Figure A.2: Image from [16], arrival time of electrons at anode.

Here it's clear to see all electrons arrive within a timespread of 5 ps. This means the time resolution of this Tipsy conifuration is 5 ps. These results need to be verified using better approximations for the energy of the TSE's, the TSEY and the angle. This can be read in the PHD thesis of Hong Wah Chan when published.

B

TSEY measurements

The maximum value for the TSEY approaches 5 which should be sufficient for Tipsy. Here all the measurement results are shown, first to compare different pulse durations for a set tynode potential. After this for a fixed pulse duration and different tynode potentials.

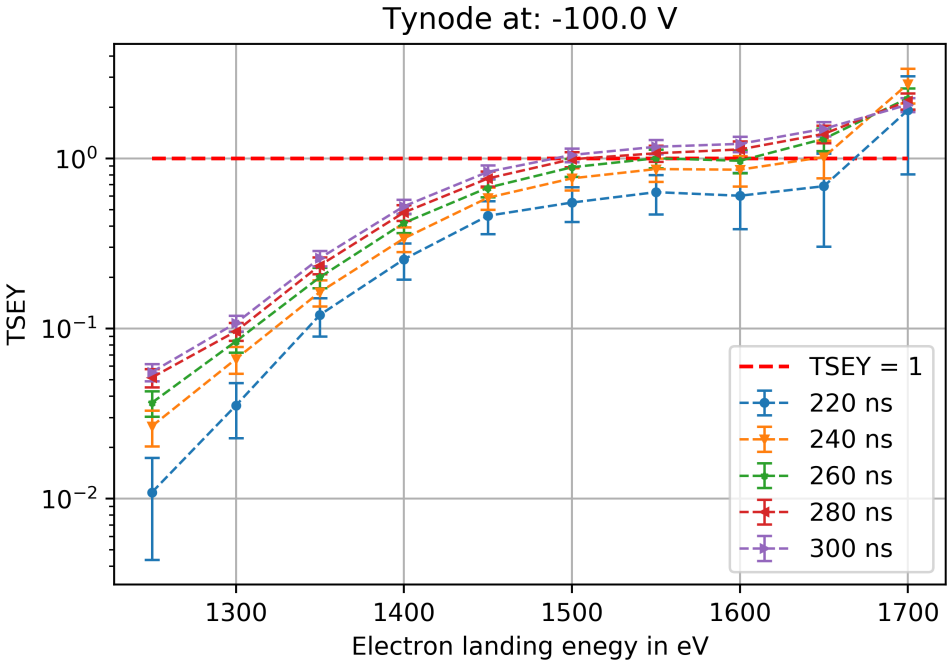

Figure B.1: Transmission yield for different pulse durations, tynode was fixed on -100 V.

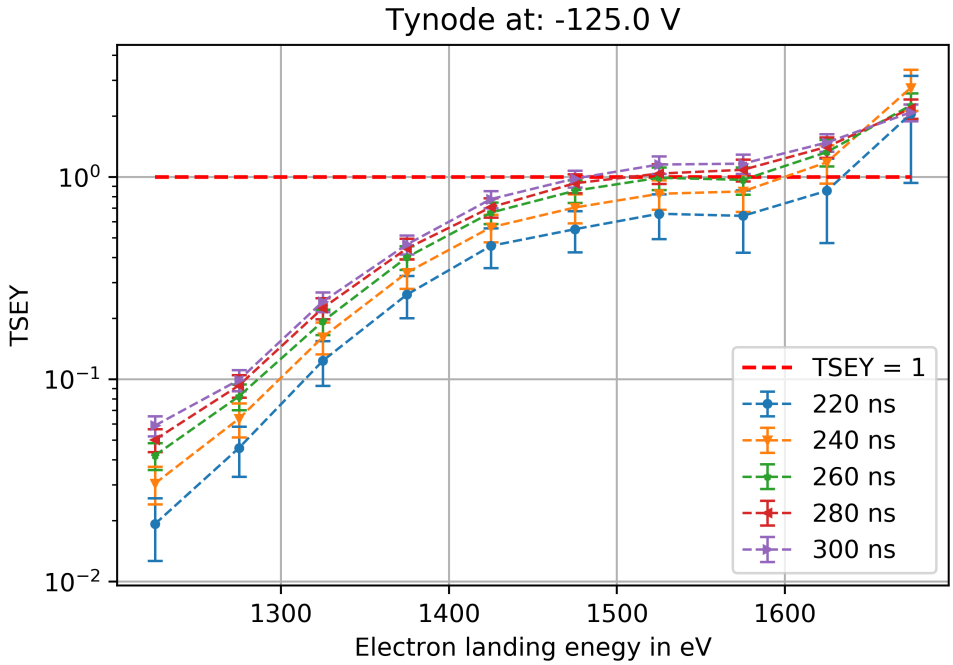

Figure B.2: Transmission yield for different pulse durations, tynode was fixed on -125 V.

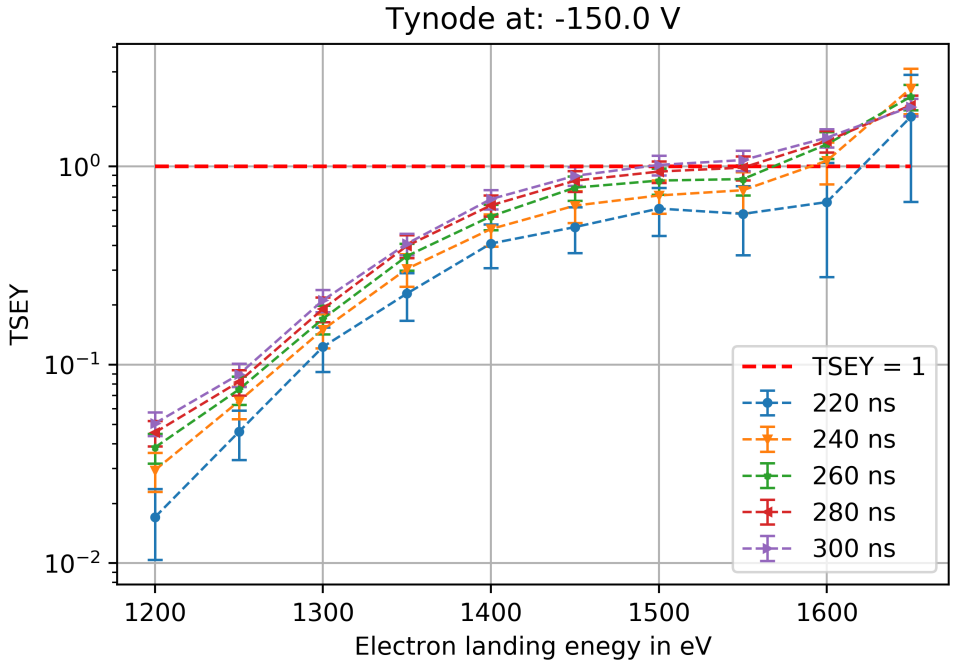

Figure B.3: Transmission yield for different pulse durations, tynode was fixed on -150 V.

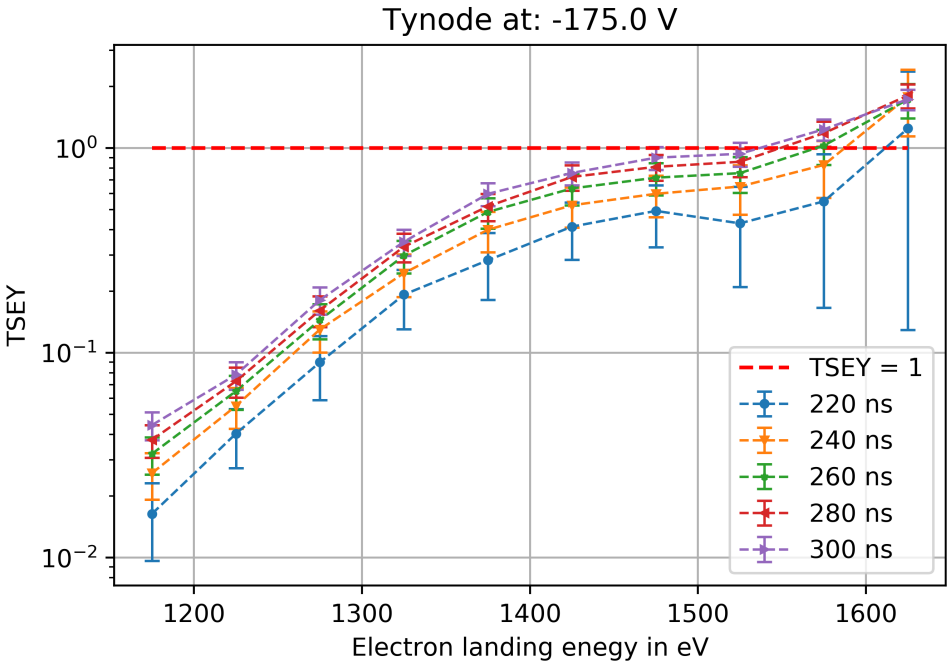

Figure B.4: Transmission yield for different pulse durations, tynode was fixed on -175 V.

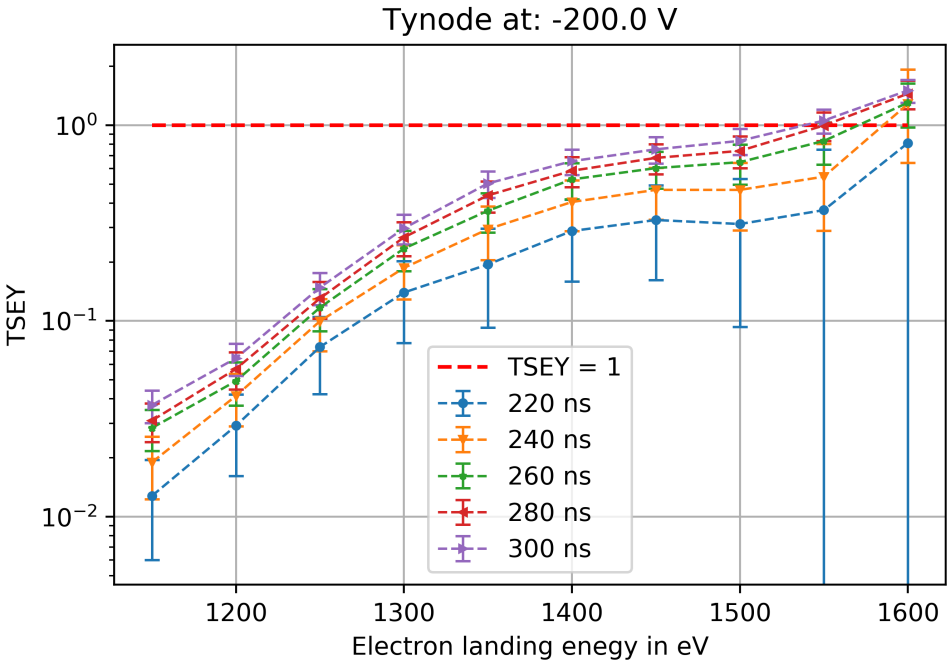

Figure B.5: Transmission yield for different pulse durations, tynode was fixed on -200 V.

If all these figures are compared we see the maximum TSEY increasing as a function of pulse duration. This can probably be explained by the size of the electron spot as shown in figure 5.11. However, the reason for the size is still unknown. Next the same data is shown but here the tynode potential is different for the same pulse duration.

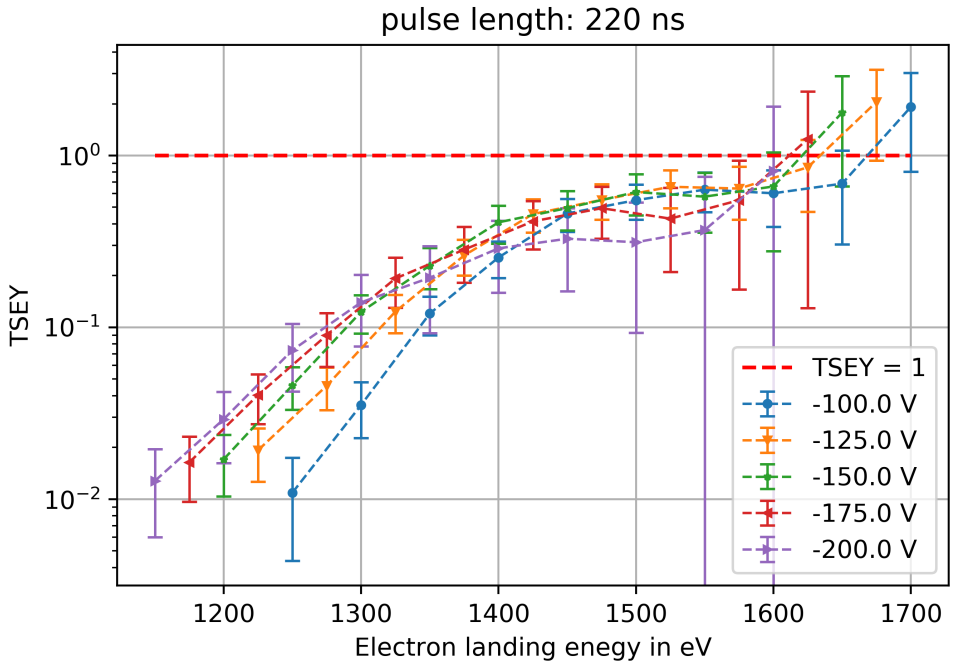

Figure B.6: TSEY measurement of a 220 ns spot for different tynode potentials.

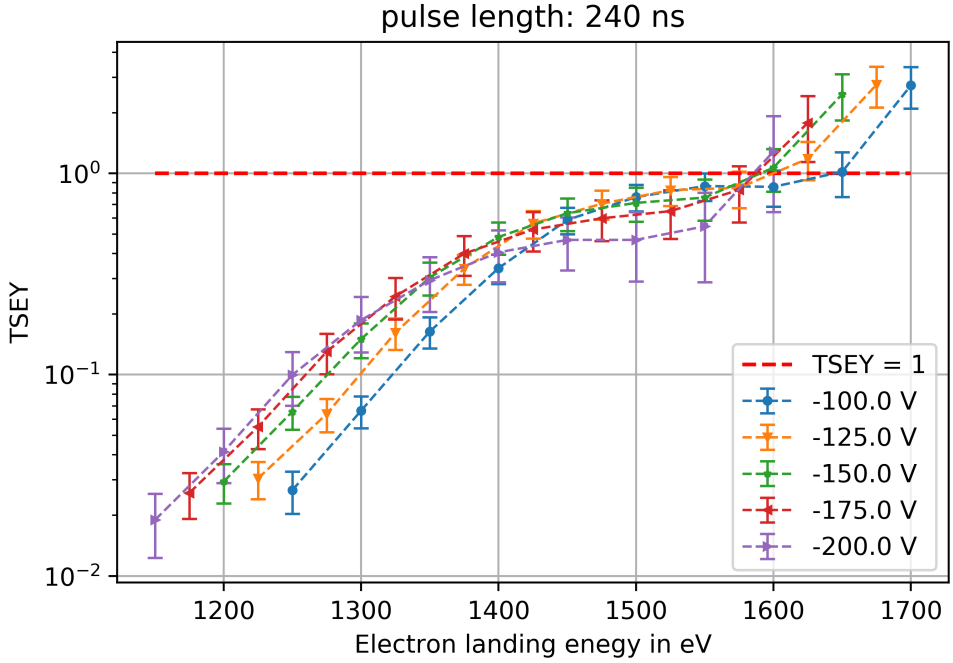

Figure B.7: TSEY measurement of a 240 ns spot for different tynode potentials.

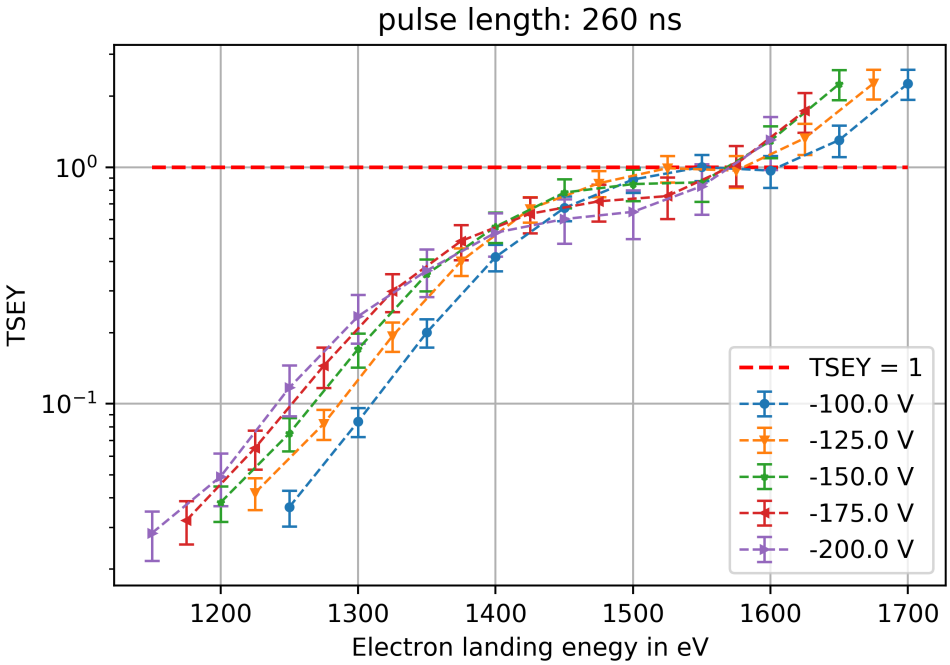

Figure B.8: TSEY measurement of a 260 ns spot for different tynode potentials.

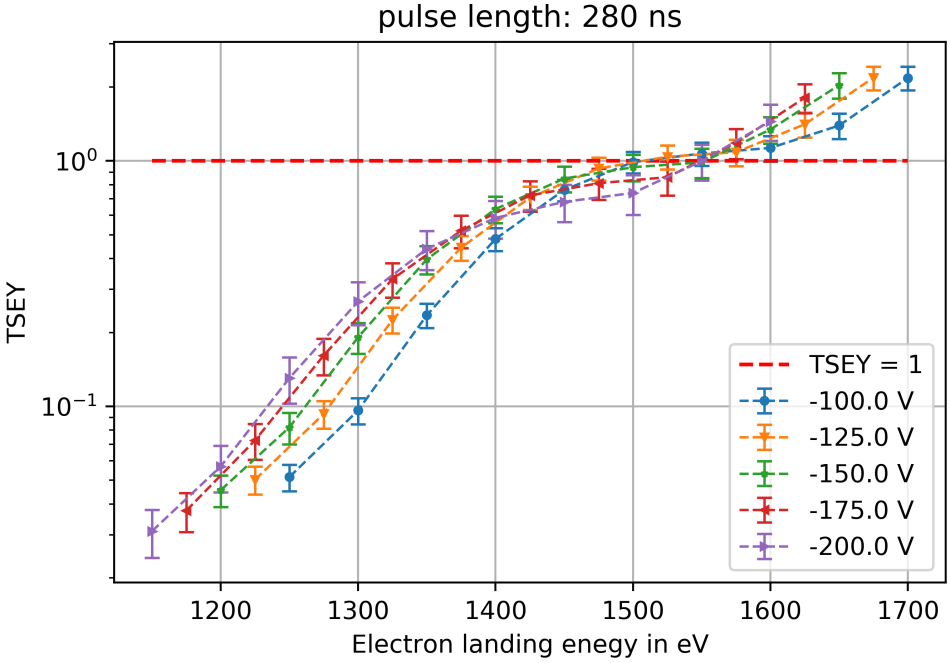

Figure B.9: TSEY measurement of a 280 ns spot for different tynode potentials.

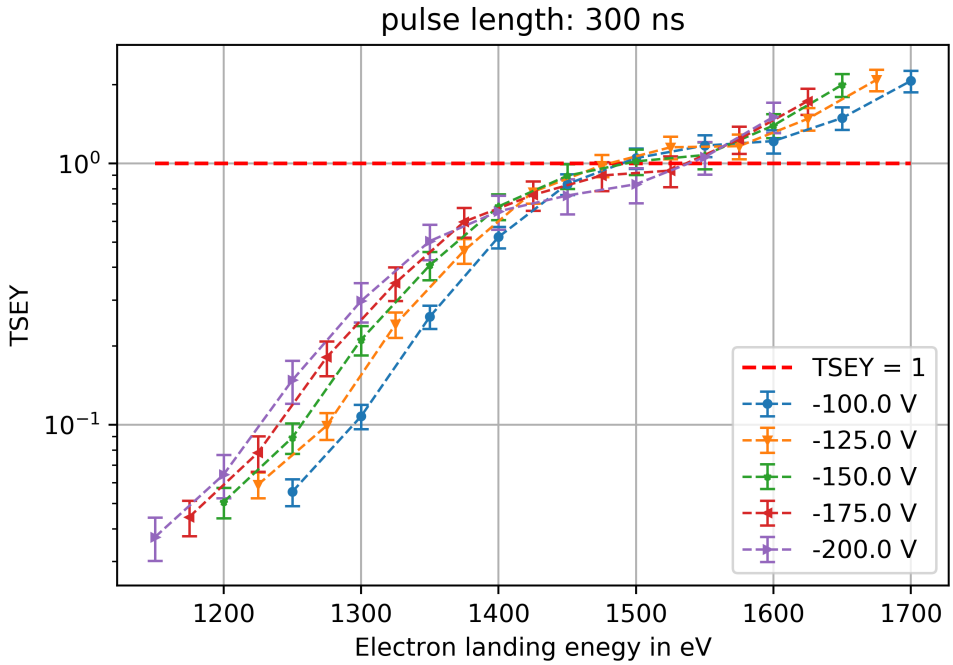

Figure B.10: TSEY measurement of a 300 ns spot for different tynode potentials.

It's interesting to see how the uncertainty decreases as the pulse duration increases. This can be explained by the increased uncertainty in the non linear part of the calibration. For a 220ns pulse duration with the tynode potential at -200 V the uncertainty seems to increase as a function of landing energy. The reason for this is still unknown.

C

Stack alignment measurements

Here the initial measurement data of the tynode alignment measurement is represented. In table C.1 the initial positions are shown. Note these absolute values don't hold information since the tynode is rotated by hand between measurements. Only the displacement in x and y can be compared for different measrue-ments.

Measurement 1. Tynode turned 0 degrees. Values in mm.

Dome	X-position T4	Y-position T4	X-position T5	Y-position T5
1	-0.0035 ± 0.004	0.0102 ± 0.004	-0.0105 ± 0.003	0.0122 ± 0.003
2	0.0461 ± 0.004	3.0357 ± 0.004	0.0421 ± 0.003	3.0387 ± 0.003
3	-2.9757 ± 0.004	3.0873 ± 0.004	-2.9833 ± 0.003	3.0911 ± 0.003
4	-3.0271 ± 0.004	0.0618 ± 0.004	-3.0371 ± 0.003	0.0678 ± 0.003

Measurement 2. Tynode turned 90 degrees clockwise. Values in mm.

Dome	X-position T4	Y-position T4	X-position T5	Y-position T5
1	-1.588 ± 0.004	6.5124 ± 0.004	-1.594 ± 0.003	6.5224 ± 0.003
2	-4.6115 ± 0.004	6.4521 ± 0.004	-4.6175 ± 0.003	6.4601 ± 0.003
3	-4.5454 ± 0.004	3.3709 ± 0.004	-4.5554 ± 0.003	3.4381 ± 0.003
4	-1.524 ± 0.004	3.4873 ± 0.004	-1.532 ± 0.003	3.4973 ± 0.003

Measurement 3. Tynode turned 180 degrees clockwise. Values in mm.

Dome	X-position T4	Y-position T4	X-position T5	Y-position T5
1	-6.0683 ± 0.004	3.6843 ± 0.004	-6.0813 ± 0.003	3.6943 ± 0.003
2	-5.9778 ± 0.004	0.6627 ± 0.004	-5.9868 ± 0.003	0.6697 ± 0.003
3	-2.952 ± 0.004	0.7531 ± 0.004	-2.965 ± 0.003	0.7631 ± 0.003
4	-3.0446 ± 0.004	3.7803 ± 0.004	-3.0596 ± 0.003	3.7873 ± 0.003

Measurement 3. Tynode turned 270 degrees clockwise. Values in mm.

Dome	X-position T4	Y-position T4	X-position T5	Y-position T5
1	-7.2598 ± 0.004	-0.1791 ± 0.004	-7.2768 ± 0.003	-0.1741 ± 0.003
2	-4.2364 ± 0.004	-0.1731 ± 0.004	-4.2474 ± 0.003	-0.1691 ± 0.003
3	-4.2399 ± 0.004	2.8541 ± 0.004	-4.2529 ± 0.003	2.8551 ± 0.003
4	-7.2665 ± 0.004	2.8467 ± 0.004	-7.2765 ± 0.003	2.8507 ± 0.003

Table C.1: Data measured with manipulator on Zeiss microscope at Nikhef in Amsterdam. Uncertainty of tynode 5 is 3 um and for tynode 4 it is 4 um.

The uncertainty is estimated considering the accuracy of the manipulator and the mechanical vibrations of the system. The mechanical vibrations were turned out to be the limiting factor. When determining the middle of a dome the image would shake around it's original position with a amplitude of ~ 2 μm. To be on the safe side the uncertainty is set at 3 μm for the upper tynode. The uncertainty of tynode 4 was set

at 4 µm since it was harder to focus on this tynode. By subtracting the X and Y positions for tynode 4 and tynode 5 the displacement in X and Y is calculated for each dome. By averaging this displacement per dome the *true* displacement cancels out. Therefore the result is the displacement caused by the re focussing of the microscope. The results are shown in table C.2, where M1 to M4 stands for measurement 1 to 4 and D1 to D4 stands for dome 1 to 4.

	D1 dx	D1 dy	D2 dx	D2 dy	D3 dx	D3 dy	D4 dx	D4 dy
M1	7.0 ± 5.0	-2.0 ± 5.0	4.0 ± 5.0	-3.0 ± 5.0	7.6 ± 5.0	-3.8 ± 5.0	10.0 ± 5.0	-6.0 ± 5.0
M2	6.0 ± 5.0	-10.0 ± 5.0	6.0 ± 5.0	-8.0 ± 5.0	10.0 ± 5.0	-12.2 ± 5.0	8.0 ± 5.0	-10.0 ± 5.0
M3	13.0 ± 5.0	-10.0 ± 5.0	9.0 ± 5.0	-7.0 ± 5.0	13.0 ± 5.0	-10.0 ± 5.0	15.0 ± 5.0	-7.0 ± 5.0
M4	17.0 ± 5.0	-5.0 ± 5.0	11.0 ± 5.0	-4.0 ± 5.0	13.0 ± 5.0	-1.0 ± 5.0	10.0 ± 5.0	-4.0 ± 5.0
Average:	10.8 ± 2.5	-6.8 ± 2.5	7.5 ± 2.5	-5.5 ± 2.5	10.9 ± 2.5	-6.8 ± 2.5	10.8 ± 2.5	-6.8 ± 2.5

Table C.2: Values are now in um, uncertainty of average is 1 standard deviation.

The first thing to note is that all displacements have the same sign, which is weird because the stack is rotated between the measurements. This means that the displacement due to refocussing the microscope is more significant compared to the *true* displacement of the tynodes. Therefore the the focussing error in the microscope is determined first. The results are shown in table 6.1 and from this is concluded that for each x and y displacement a mistake of 9.97 ± 1.65 and -6.43 ± 0.62 µm is made respectively. Therefore these values are subtracted from the measurements shown in table C.3.

	D1 dx	D1 dy	D2 dx	D2 dy	D3 dx	D3 dy	D4 dx	D4 dy
M1	3.0 ± 5.2	4.4 ± 5.2	6.0 ± 5.2	3.4 ± 5.2	2.4 ± 5.2	2.6 ± 5.2	0.0 ± 5.2	0.4 ± 5.2
M2	3.6 ± 5.2	4.0 ± 5.2	1.6 ± 5.2	4.0 ± 5.2	5.8 ± 5.2	0.0 ± 5.2	3.6 ± 5.2	2.0 ± 5.2
M3	3.0 ± 5.2	3.6 ± 5.2	-1.0 ± 5.2	0.6 ± 5.2	3.0 ± 5.2	3.6 ± 5.2	5.0 ± 5.2	0.6 ± 5.2
M4	1.4 ± 5.2	7.0 ± 5.2	2.4 ± 5.2	1.0 ± 5.2	5.4 ± 5.2	3.0 ± 5.2	2.4 ± 5.2	0.0 ± 5.2
Average:	2.7 ± 0.9	4.7 ± 1.6	2.2 ± 2.9	2.3 ± 1.7	4.1 ± 1.7	2.3 ± 1.6	2.3 ± 2.1	0.8 ± 0.8

Table C.3: Values in um. In this table the rotation of the stack is taken into account. For example, a negative horizontal displacement will be a positive vertical displacement after a rotation of 90 degrees. After this the average is taken.

From this data table 6.2 is created, which leads to a average displacement of 4.1 ± 1.3 µm.

Bibliography

[1] Harry van der Graaf, Michiel Bakker, Hong Wah Chan, Edoardo Charbon, Fabio Santagata, Pasqualina Sarro, and Dennis Schaart. The tipsy single soft photon detector and the trixy ultrafast tracking detector. In *2012 IEEE Nuclear Science Symposium and Medical Imaging Conference Record (NSS/MIC)*, pages 1952–1956. IEEE, 2012.

[2] Sense. Photomultiplier tubes (pmt). `https://www.sense-pro.org/lll-sensors/pmt`, Unknown. Accessed: 2018-05-24.

[3] HAMAMATSU PHOTONICS. *PHOTOMULTIPLIER TUBES, Basics and Applications*, 2007.

[4] Jin Pyo Lee, Mikiko Ito, and Jae Sung Lee. Evaluation of a fast photomultiplier tube for time-of-flight pet. *Biomedical Engineering Letters*, 1(3):174, Sep 2011.

[5] Joseph Ladislas Wiza et al. Microchannel plate detectors. *Nucl. Instrum. Methods*, 162(1-3):587–601, 1979.

[6] V. Prodanovic. *Ultra-thin mems fabricated tynodes for electron multiplication*. PhD thesis, Delft University of Technology, 2019.

[7] GW Fraser. X-and gamma-ray imaging using microchannel plates. *Nuclear Instruments and Methods in Physics Research*, 221:115–130, 1984.

[8] T. Gys. Micro-channel plates and vacuum detectors. *Nuclear Instruments and Methods in Physics Research Section A: Accelerators, Spectrometers, Detectors and Associated Equipment*, 787:254 – 260, 2015. New Developments in Photodetection NDIP14.

[9] Slawomir S. Piatek. Photonics products: Photodiodes: Silicon low-light photodiodes don't miss a photon. `https://hub.hamamatsu.com/jp/en/technical-note/how-sipm-works/index.html`, 2016. Accessed: 2019-11-20.

[10] SensL. Introduction to sipm technical note. Technical report, SENSL, 2011.

[11] Bernicy S Fong, Murray Davies, and Pierre Deschamps. Timing resolution and time walk in slik spad: measurement and optimization. In *Optical Sensing, Imaging, and Photon Counting: Nanostructured Devices and Applications 2017*, volume 10353, page 1035309. International Society for Optics and Photonics, 2017.

[12] Claudio Piemonte and Alberto Gola. Overview on the main parameters and technology of modern silicon photomultipliers. *Nuclear Instruments and Methods in Physics Research Section A: Accelerators, Spectrometers, Detectors and Associated Equipment*, 926:2 – 15, 2019. Silicon Photomultipliers: Technology, Characterisation and Applications.

[13] Patrick Eckert, Hans-Christian Schultz-Coulon, Wei Shen, Rainer Stamen, and Alexander Tadday. Characterisation studies of silicon photomultipliers. *Nuclear Instruments and Methods in Physics Research Section A: Accelerators, Spectrometers, Detectors and Associated Equipment*, 620(2-3):217–226, 2010.

[14] Harry van der Graaf, Hassan Akhtar, Neil Budko, Hong Wah Chan, Cornelis W Hagen, Conny CT Hansson, Gert Nützel, Serge D Pinto, Violeta Prodanović, Behrouz Raftari, et al. The tynode: A new vacuum electron multiplier. *Nuclear Instruments and Methods in Physics Research Section A: Accelerators, Spectrometers, Detectors and Associated Equipment*, 847:148–161, 2017.

[15] Marcus Ossiander, Johann Riemensberger, S Neppl, M Mittermair, Martin Schäffer, A Duensing, MS Wagner, R Heider, M Wurzer, M Gerl, et al. Absolute timing of the photoelectric effect. *Nature*, 561(7723):374, 2018.

[16] Hong Wah Chan. *Not yet published*. PhD thesis, TU Delft, University of technology and Nikhef Amsterdam, Expected in 2020.

[17] RC Alig and S Bloom. Electron-hole-pair creation energies in semiconductors. *Physical review letters*, 35(22):1522, 1975.

[18] Robert G. Lye and A. J. Dekker. Theory of secondary emission. *Phys. Rev.*, 107:977–981, Aug 1957.

[19] L Reimer. Scanning electron microscopy: Physics of image formation and microanalysis, second edition. *Measurement Science and Technology*, 11(12):1826–1826, nov 2000.

[20] Thomas Verduin. *Quantum noise effects in e-Beam Lithography and Metrology*. PhD thesis, TU Delft, University of technology, 2017.

[21] EJ Sternglass and MM Wachtel. Transmission secondary electron multiplication for high-speed pulse counting. *IRE Transactions on Nuclear Science*, 3(4):29–32, 1956.

[22] Shu Xia Tao, Hong Wah Chan, and Harry Van Der Graaf. Secondary electron emission materials for transmission dynodes in novel photomultipliers: a review. *Materials*, 9(12):1017, 2016.

[23] N.S. Xu and S. Ejaz Huq. Novel cold cathode materials and applications. *Materials Science and Engineering: R: Reports*, 48(2):47 – 189, 2005.

[24] Hua Qin, Hyun-Seok Kim, Robert H Blick, Michael S Westphall, and Lloyd M Smith. Subthreshold field emission from thin silicon membranes. *Applied Physics Letters*, 91(18):183506, 2007.

[25] Hua Qin, Renbing Tan, Jonghoo Park, Hyun-Seok Kim, and Robert H Blick. Direct observation of subthreshold field emission from silicon nanomembranes. *Journal of Applied Physics*, 109(12):124504, 2011.

[26] Thijs ten Bruggencate. Transferred graphene as a conductive layer on a thin alumina membrane. diploma thesis, Delft University of Technology, 2019.

[27] Kazuyoshi Akiba et al. Charged Particle Tracking with the Timepix ASIC. *Nucl. Instrum. Meth.*, A661:12, 2012.

[28] Xavier Liopart. *TIMEPIX Manual v1.0*, August 2006.

[29] X. Llopart, R. Ballabriga, M. Campbell, L. Tlustos, and W. Wong. Timepix, a 65k programmable pixel readout chip for arrival time, energy and/or photon counting measurements. *Nuclear Instruments and Methods in Physics Research Section A: Accelerators, Spectrometers, Detectors and Associated Equipment*, 581(1):485 – 494, 2007. VCI 2007.

[30] Kimball Physics. *ELG-2/EGPS-1022 ELECTRON GUN and POWER SUPPLY SYSTEM*, December 2012.

[31] Wouter Landgraaf. Development of the dytest setup- as system to probe the transmission secondary electron yield of ultra-thin membranes. Master's thesis, TU Delft, the Netherlands, 2017.

[32] Hans Verkooijen. *Manual Nikhef Pulse Generator*, 2017.

[33] Jan Jakubek, Andrea Cejnarova, Tomas Holy, Stanislav Pospisil, Josef Uher, and Zdenek Vykydal. Pixel detectors for imaging with heavy charged particles. *Nuclear Instruments and Methods in Physics Research Section A: Accelerators, Spectrometers, Detectors and Associated Equipment*, 591(1):155–158, 2008.